Observation of a toroidal acoustic mode in a current-less toroidal device

Umesh Kumar

Collab:- R. Ganesh, K. Sathyanarayana and Y. C. Saxena

Institute for Plasma Research, Gandhinagar, India

Introduction

- Geodesic Acoustic Modes (GAMs) are pressure oscillations supported by plasma compressibility in a toroidal magnetic geometry where average geodesic curvature provides a restoring force.

- It is believed that GAMs interacts weakly with background turbulence and help realize a quasi-stable equilibrium in Tokamaks.

- In collision-less plasmas GAMs get damped in Tokamaks due to Landau damping. Collisions also damp GAMs.

- GAMs can be driven unstable in Tokamaks by non-linear Reynolds stress **(Itoh, 2005)** or by suprathermal ions **(Nazikian, 2008).**

- GAMs exhibit $(m = 1, n = 0)$ for density fluctuation and $(m = 0,\ n = 0)$ for potential fluctuation, where m, n are poloidal and toroidal mode number respectively.

- $f_{GAM} = \frac{c_s}{2\pi R}\sqrt{2 + \frac{1}{q^2}}$; where c_s is ion acoustic speed, R is the major radius, $1/q$ is the magnetic rotational transform and $q \propto 1/I_{tor}$ [**Itoh, 2005**].

Geodesic Acoustic mode (GAM)

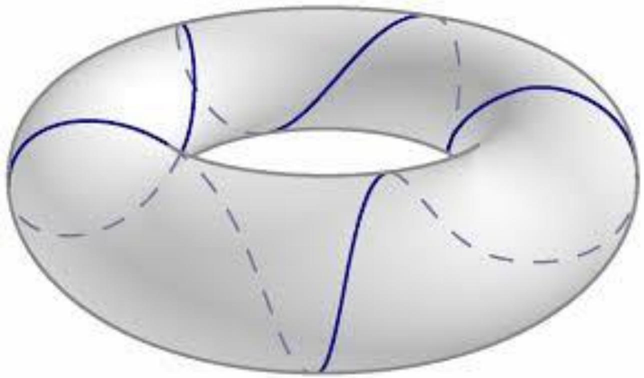

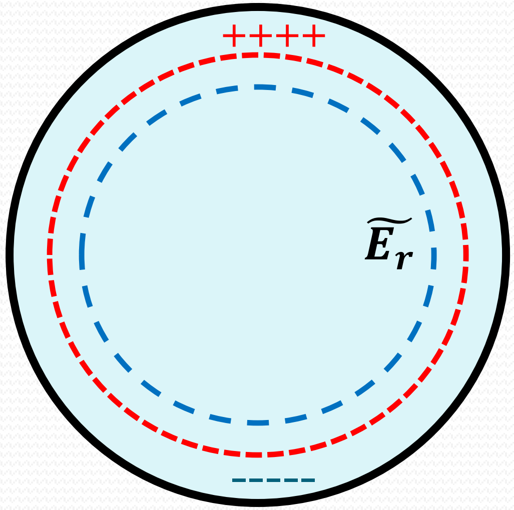

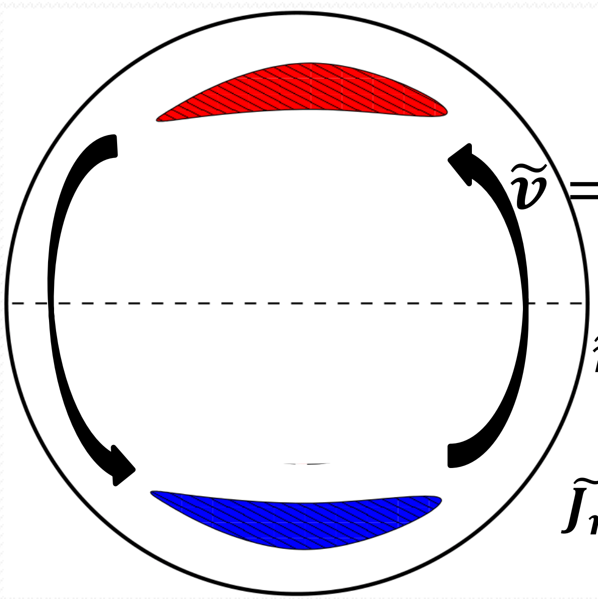

$$\widetilde{v} = \frac{\widetilde{E_r} \times B}{|B|^2}$$

$$\widetilde{n} \propto -\nabla . \widetilde{v}$$

$$\widetilde{J_r} \propto \frac{B \times \nabla \widetilde{n}}{|B|^2}$$

$$t + \frac{T_{GAM}}{2}$$

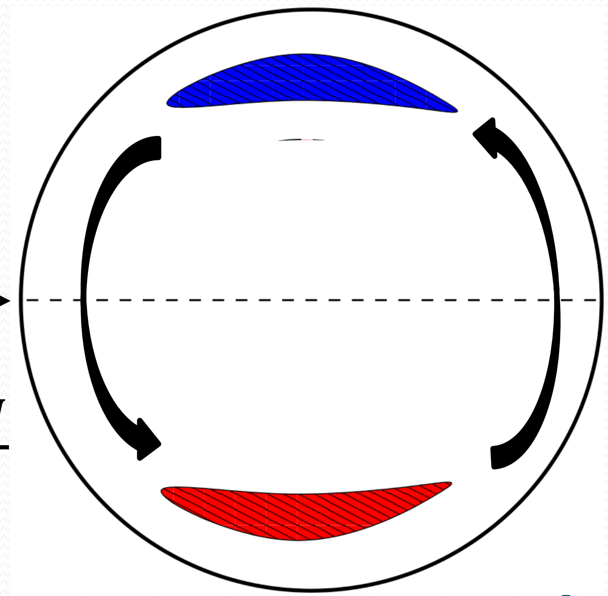

Motivation

- In a current-less toroidal device (CTD), I_{tor} is negligible. Plasma is confined only by the application of toroidal magnetic field and/or vertical magnetic field.
- In a CTD, effective rotational transform cease to exist, it implies, $q \rightarrow \infty$ and $f_{GAM} = \frac{\sqrt{2}c_s}{2\pi R}$ and no Geodesic Acoustic mode is possible.
- Is it possible to drive an acoustic mode by a regular curvature in plasmas confined by open magnetic field lines?
- In the present work, we attempted to experimentally investigate possibility of acoustic mode in a CTD with GAM-like structures in a nearly collision-less regime.

Currentless toroidal device and Tokamak

Schematic of a Tokamak

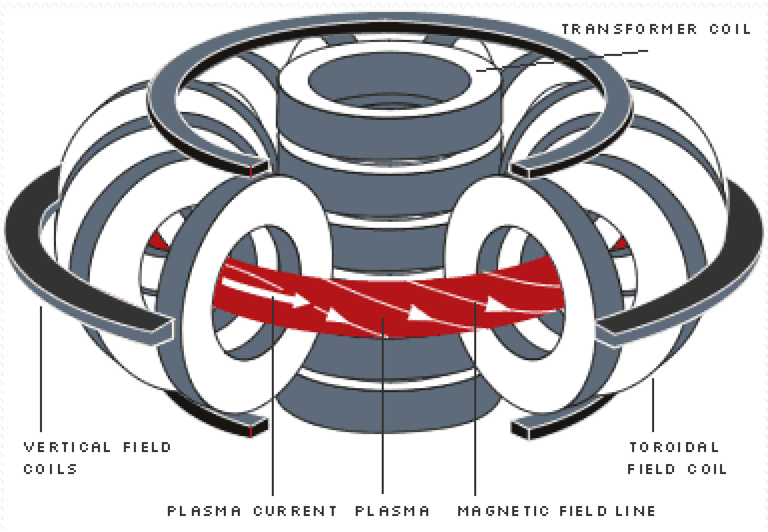

- Tokamak has a toroidal current which provides poloidal magnetic field.
- The net magnetic field is helical in nature.

Schematic of a CTD

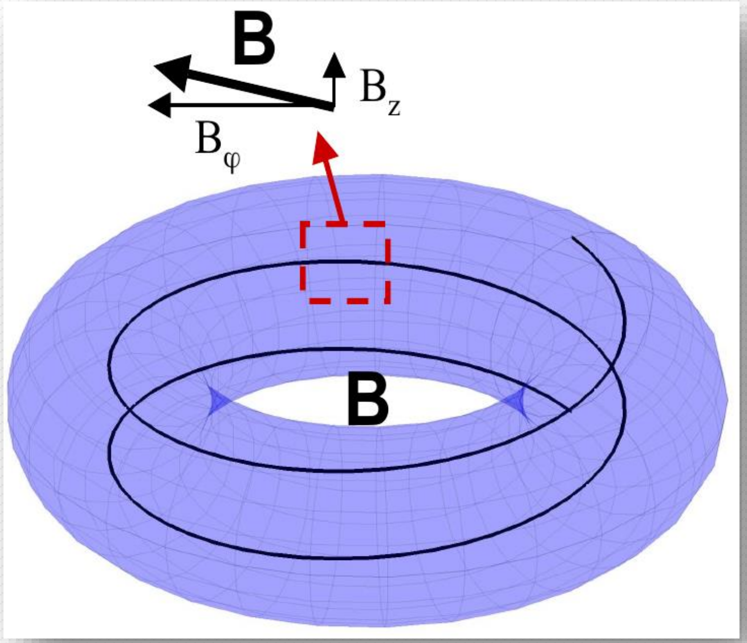

- CTD has no toroidal plasma current.
- The net magnetic field is resultant due toroidal and vertical magnetic fields.
- Image courtesy **F. Poli (2007)**

Role of vertical magnetic field

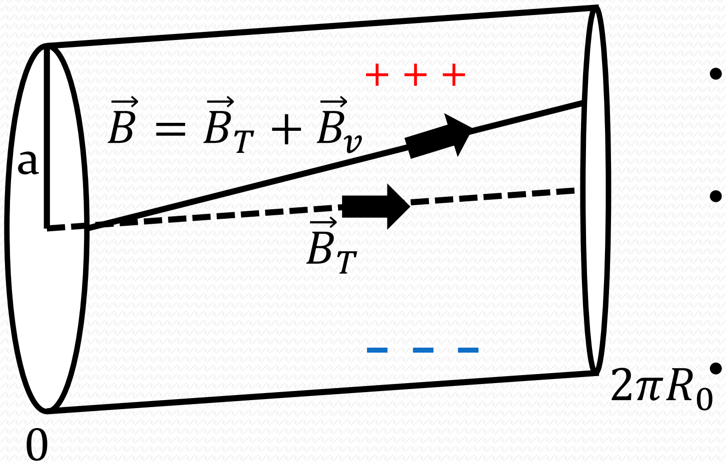

- Schematic showing torus cut open as a cylinder.
- Due to $\vec{B}_v$, the field lines are slightly shifted in vertical direction.
- Electrons follow the resultant field and help in short circuiting the E_z.

- E_z is estimated by equating toroidal magnetic drift to the vertical velocity of the electron. [**Nakao et al (1983)**], leading to:

$$\mathrm{v}_{\mathrm{E_z} \times B} = \frac{T_e m_e \nu_{en}}{e^2 R B_v^2}$$

$$\tau_C = \frac{a}{v_{E_z \times B}}$$

where τ_C is single particle confinement time and a is the minor radius of torus.

- Therefore as B_v increases confinement time increases, which can result in higher plasma density.

Experimental assembly, BETA

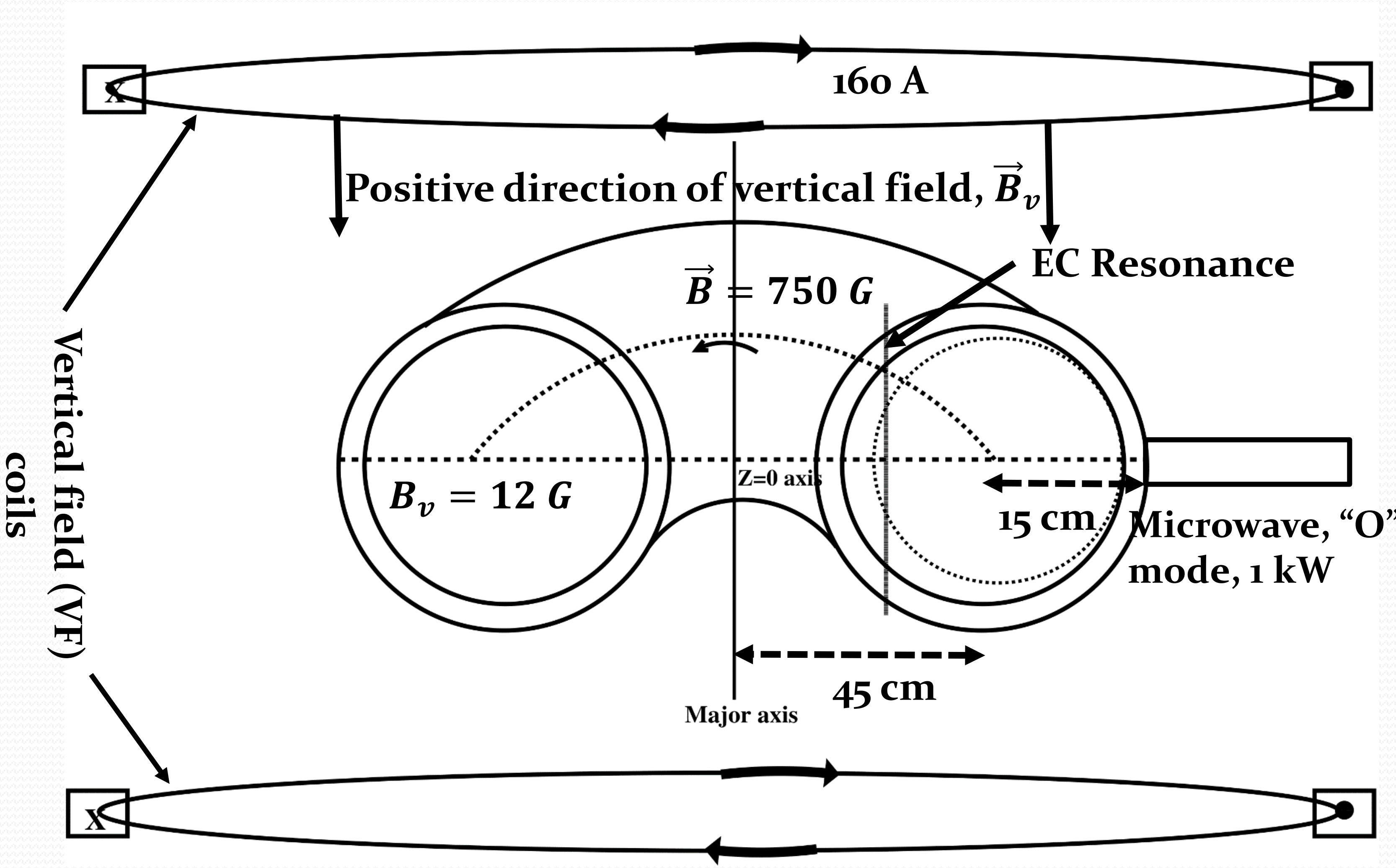

Mode number measurement

- R1 and R2 assembly provides toroidal mode number, “n”.
- TP and BP assembly provides poloidal mode number “m”.
- (b) GAM mode density fluctuation.
- Red indicates compression and blue indicates expansion due to GAM phase velocity.

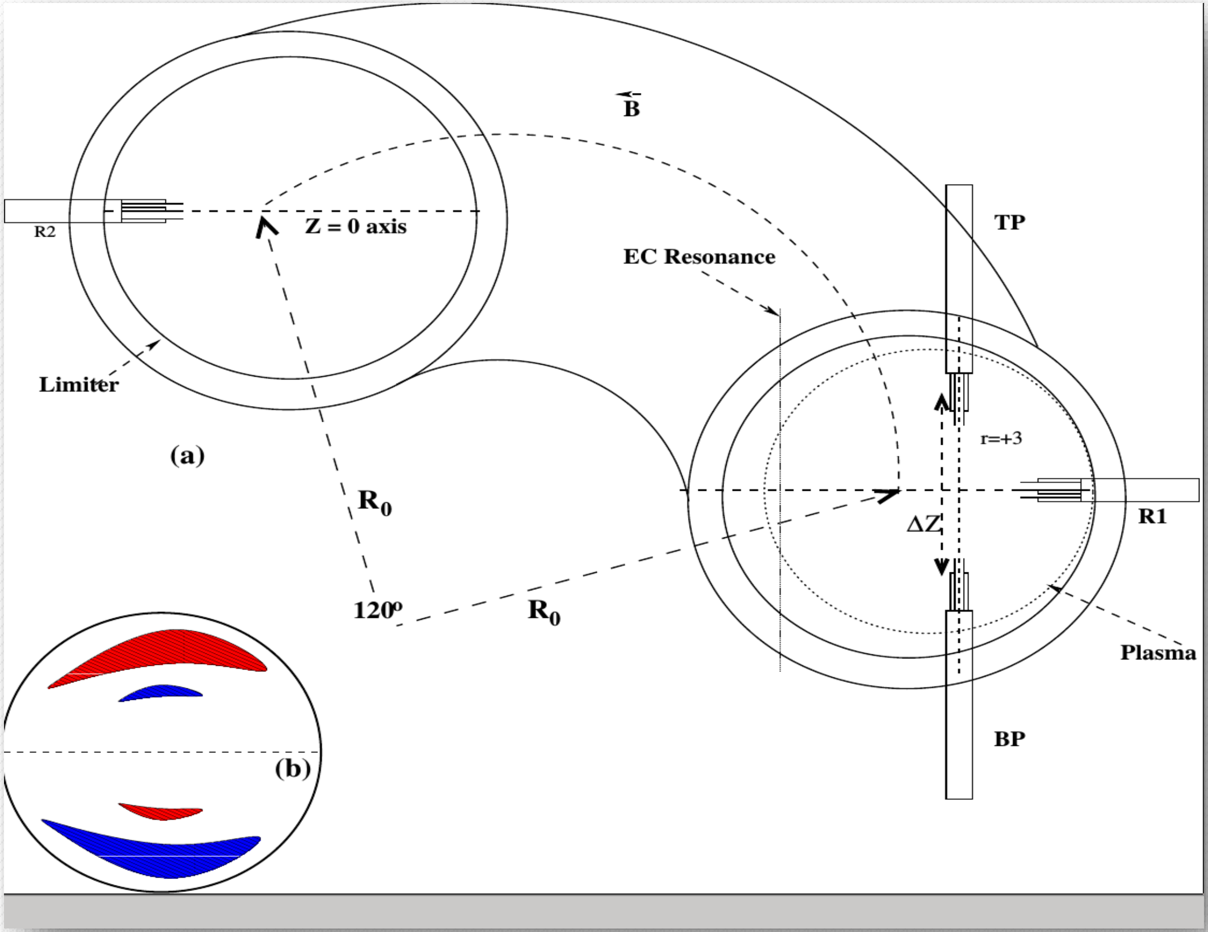

Experimental profiles

- Langmuir probes have been used to measure plasma parameters such as density, electron temperature, plasma potential and floating potential.

- Primary ionization is caused by the ECR at -6 cm and unspent energy reflects from wall to produce secondary ionization due to upper hybrid resonance.

- Experimental detection of the TAM mode is performed for three different gases viz., Neon, Argon and Krypton.

- Let us first discuss the results of Argon plasma in detail.

Density, electron temperature and UH resonance for Argon plasma

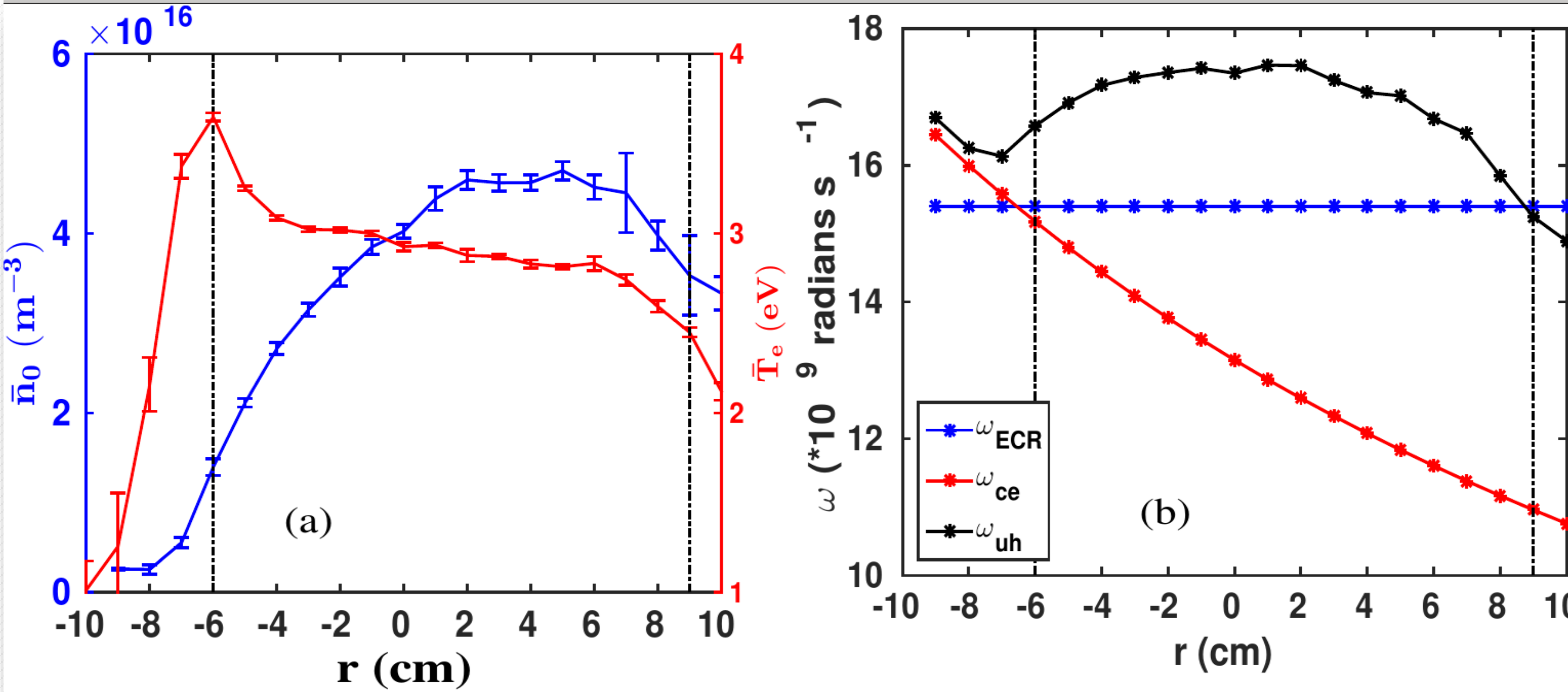

- The profile of (a) mean density ($\bar{n}_0$) and mean electron temperature ($\overline{T_e}$) and (b) upper hybrid resonance, $\omega_{UH}^2(r) = \omega_{ce}^2(r) + \omega_{pe}^2(r)$.
- Here gradients in ($\bar{n}_0$) and ($\overline{T_e}$) are weak for the region of +1 cm to +6 cm, then scale length changes beyond +7 cm.

Plasma potential and net poloidal flow

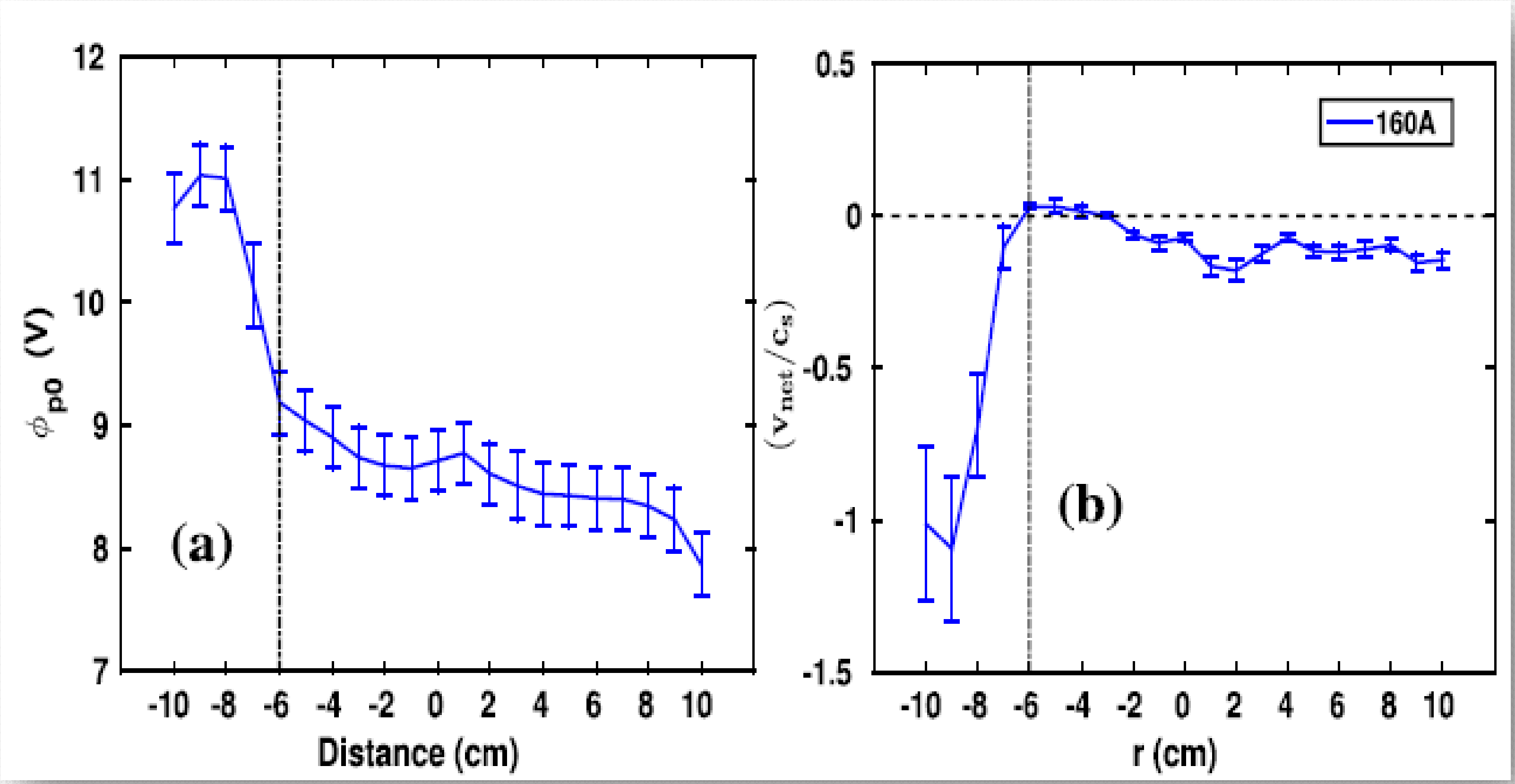

- (a) The radial profile of mean plasma potential (ϕ_{p0}) and (b) the net poloidal flow measured using the Mach probe.
- The EC resonance is shown by a vertical line in (a), which coincides with the peak in the location of electron temperature.

Nature of modes for Argon plasma

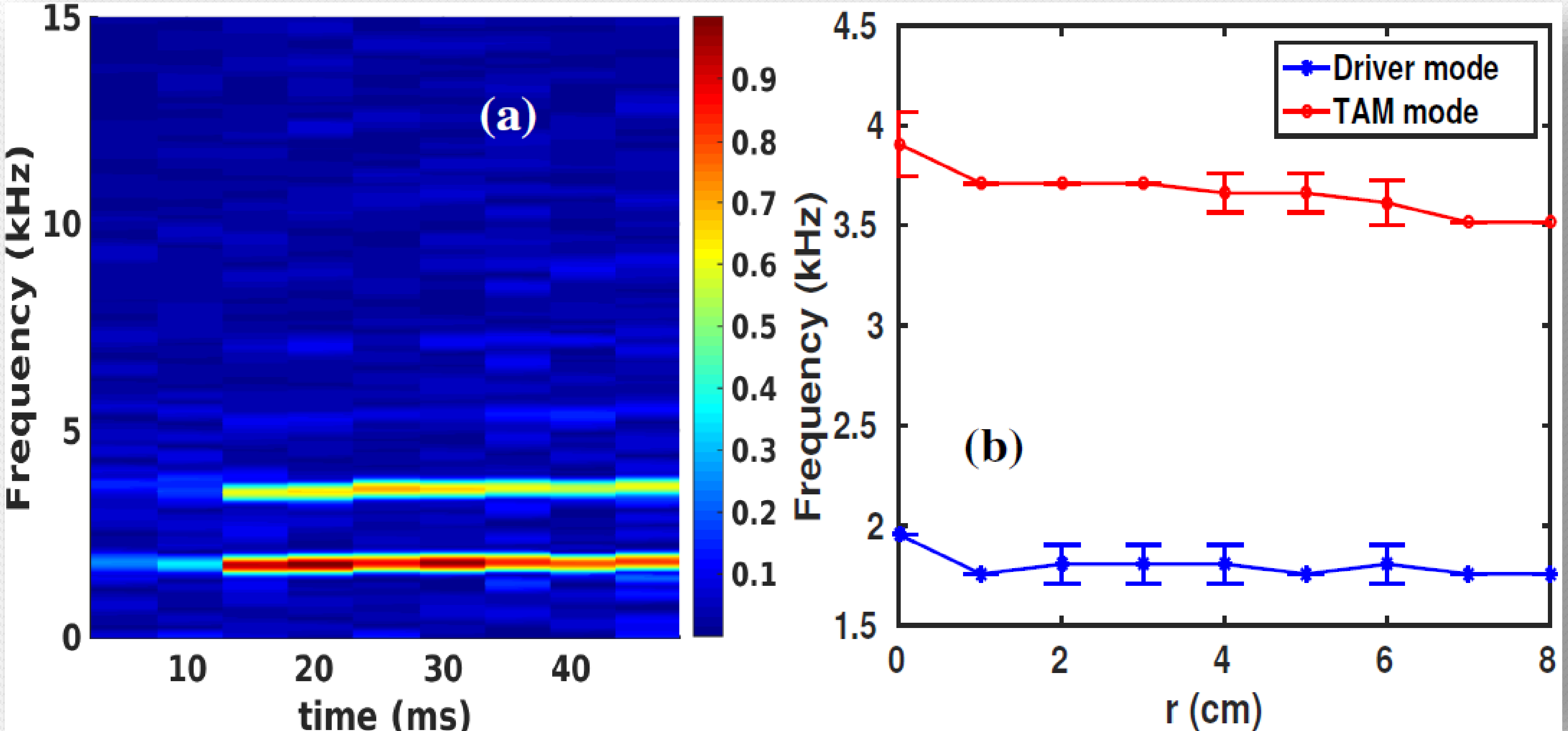

- Spectrogram of density fluctuation and radial variation of the observed modes for Argon plasma.
- The spontaneously generated driver mode shows interchange like properties (i.e., $\theta_{n\phi} \approx \pi$), has frequency $f_{driver} = 1.4\sqrt{2}c_s/(2\pi R)$=1.7 kHz .
- The TAM mode excites after, the driver mode achieves its full strength. The frequency of TAM is $f_{TAM} = 3\sqrt{2}c_s/(2\pi R)$=3.4 kHz

Toroidal mode number determination for Argon plasma

Density fluctuation

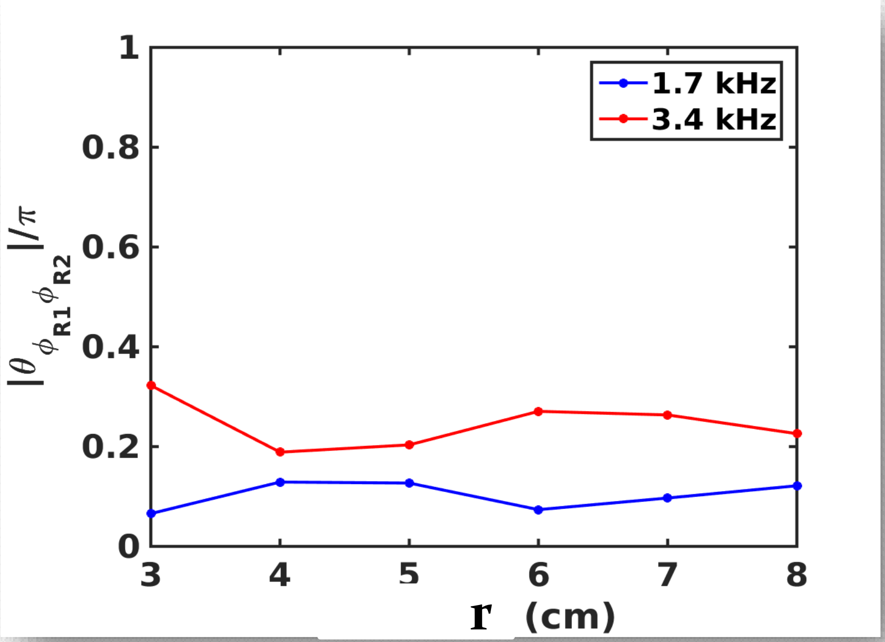

Potential fluctuation

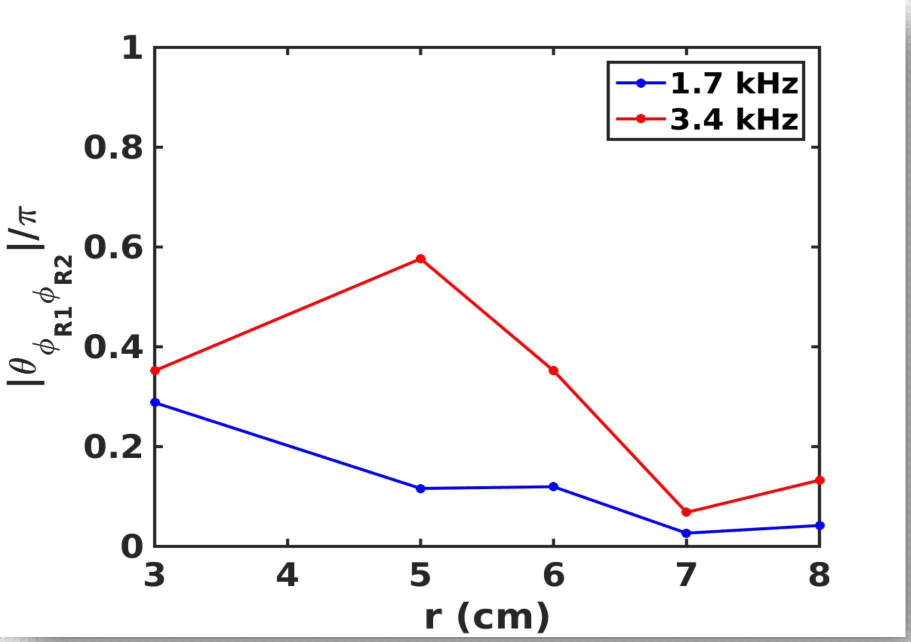

- If toroidal wavelength, $\lambda_{tor} = \frac{2\pi\Delta x}{\Delta\theta} \gg 2\pi R \implies n = 0$; where Δx is toroidal probe separation and $\Delta\theta$ is the measured phase difference.
- Coherence, $\gamma \geq 0.8$, for all cases (not shown here).
- These error-bars are not shown for these measurements.

poloidal mode number determination for Argon plasma

Density fluctuation

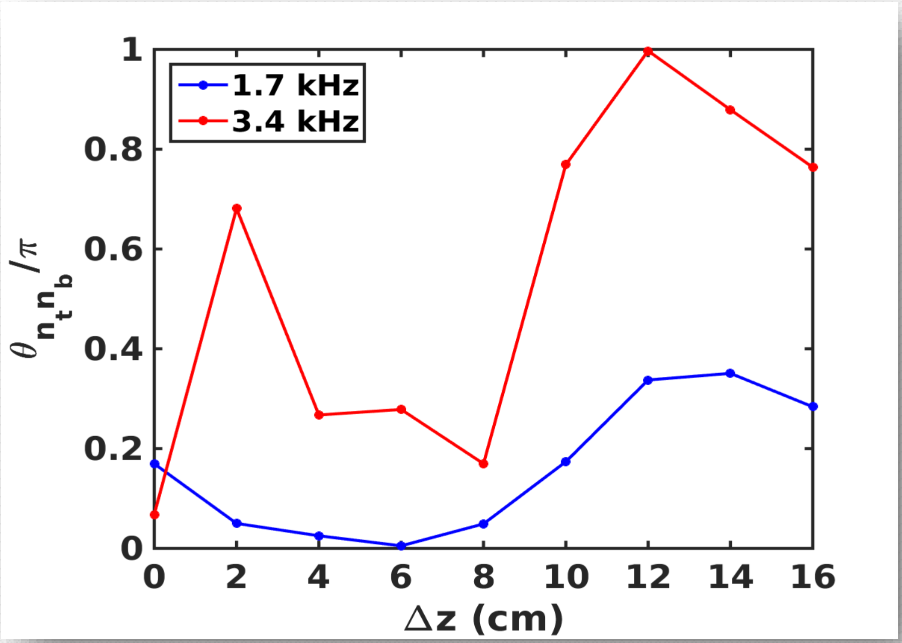

Potential fluctuation

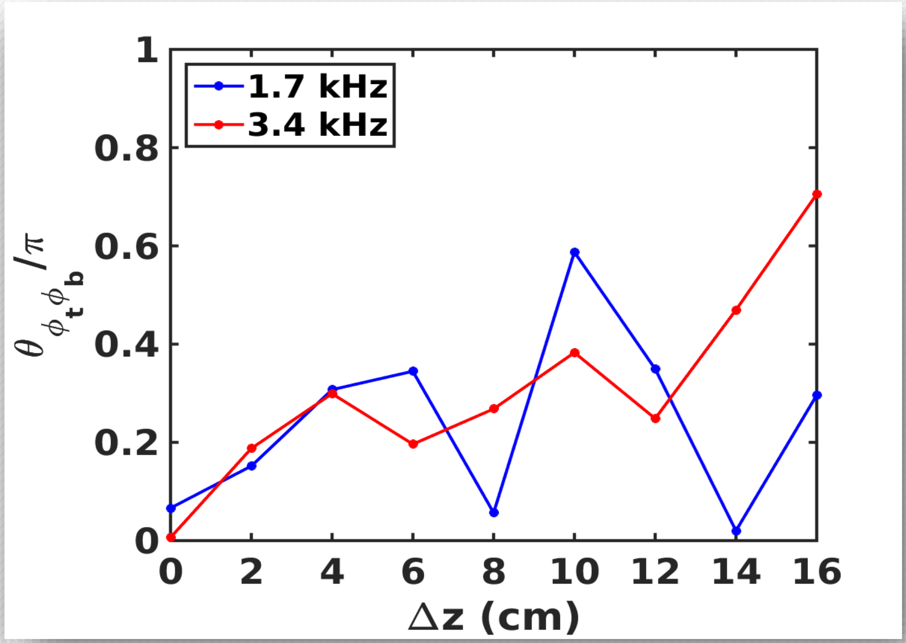

- The phase for density fluctuation for 3.4 kHz is 0.8π or more beyond $\Delta Z = 10cm$.
- Coherence > 0.8 and for potential phase varied from 0.2π to 0.7π in the same region.
- These error-bars are not shown for these measurements.

Non-linear interaction of density fluctuation at r=+5 cm

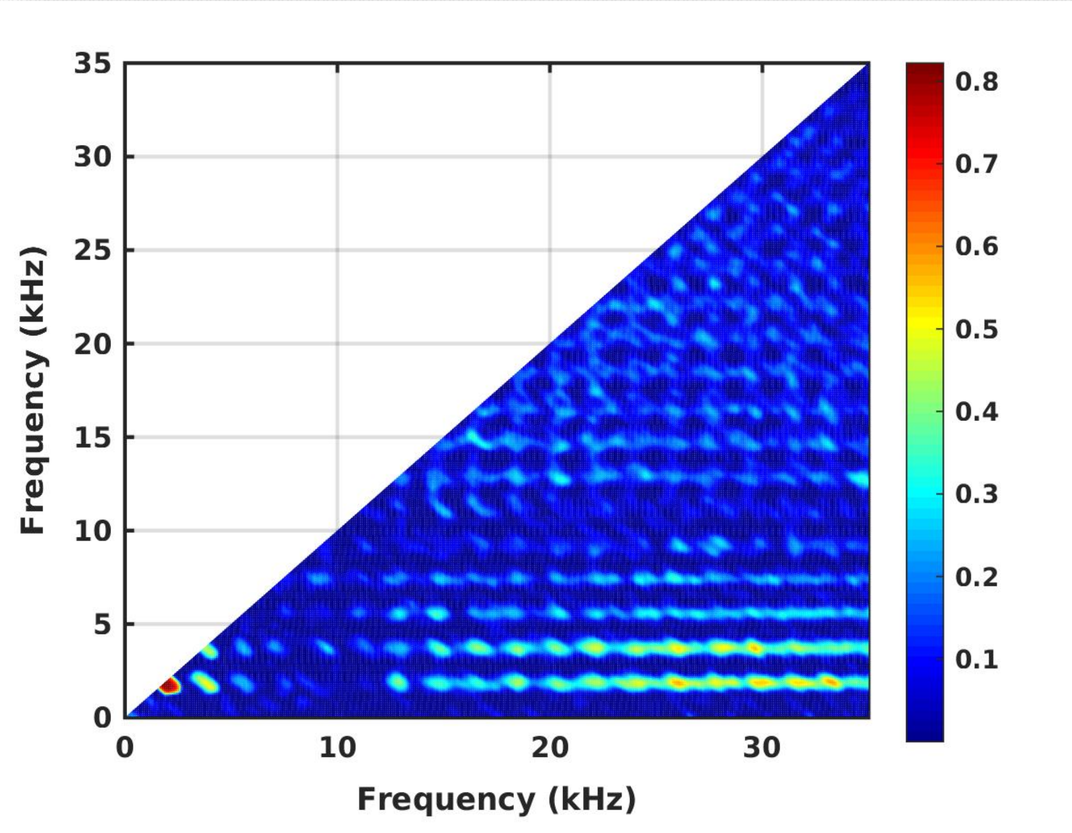

- The driver mode at 1.7 kHz interacts with itself.
- It implies that the 3.4 kHz peak is due to the self non-linear interaction of the 1.7 kHz.
- Presence of low amplitude background fluctuations is visible for frequencies beyond 20 kHz.

Variation of mode frequencies with ion mass

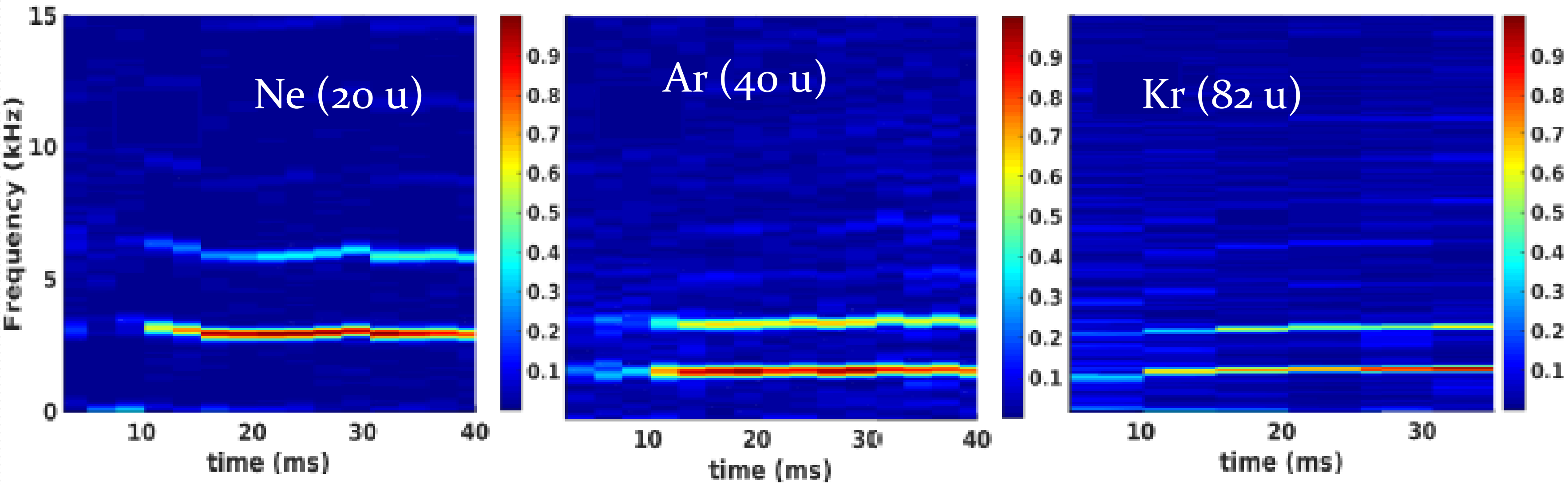

- In order to confirm the acoustic-like nature ($f_{TAM} \propto 1/\sqrt{M_i}$) of the observed mode, the ion mass has varied.
- Both the driver and TAM modes exist for all the ion masses and exhibit acoustic nature.

Variation of frequency of the observed modes with the ion mass

- The error-bars are due to frequency resolution and shot to shot variation in the frequency.
- A dashed black line has been added to aid the view.
- Thus demonstrating the Acoustic nature of both the modes.

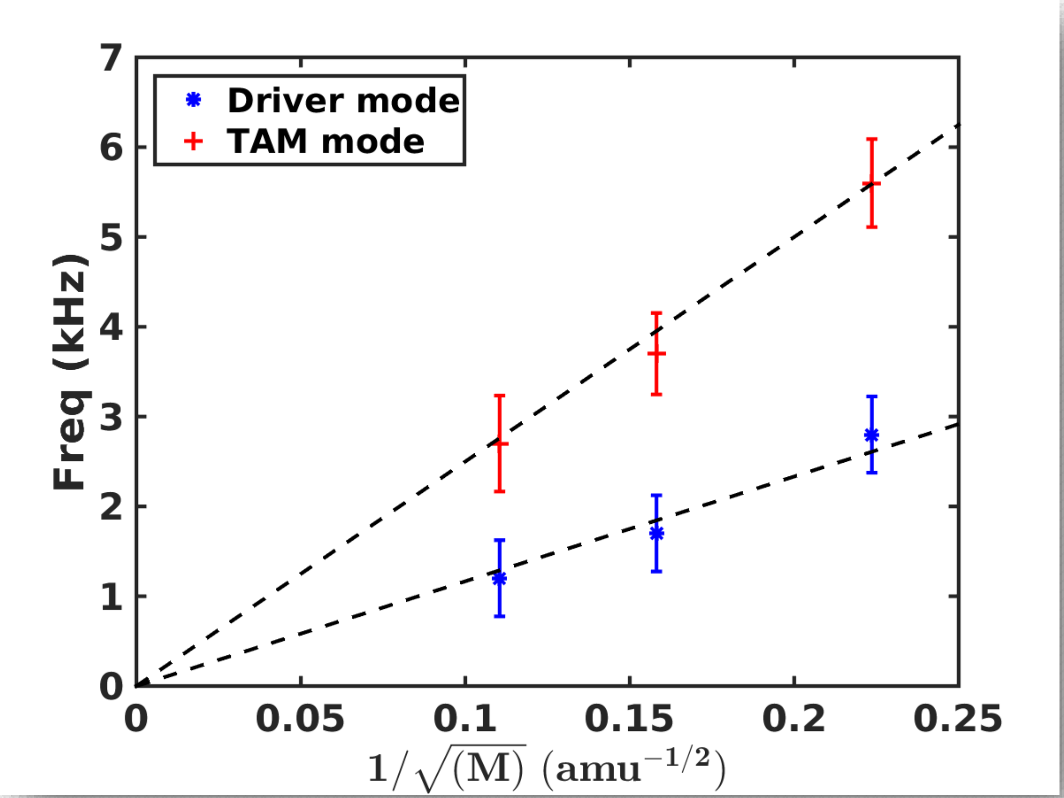

Summary

Characteristics	Driver Mode	TAM
Generation	Not clear (spontaneously generated)	Generated by non-linear interaction of driver mode with itself
Radial variation	Global, discrete	Global, discrete
Frequency	$\sim 1.4\frac{\sqrt{2}c_s}{2\pi R}$	$\sim 3\frac{\sqrt{2}c_s}{2\pi R}$
Mode characteristics	$m \geq 0, n = 0$ (for both density as well as potential fluctuation)	$m \geq 0, n = 0$ (for potential fluctuation) $m = 1, n = 0$ (for density fluctuation)
Acoustic nature	$freq \propto \frac{1}{\sqrt{M_i}}$	$freq \propto \frac{1}{\sqrt{M_i}}$
Nonlinear interaction	Interact with itself and background turbulence	Interact with background turbulence
Nature	Interchange like ($\theta_{n\phi} \sim \pi$), exact nature not known	Analogous to GAM often observed in Tokamak

Conclusion

- A discrete, global TAM mode is observed in a simple toroidal device for the very first time.
- The frequency of the observed TAM mode is almost three times that of theoretical GAM frequency for a CTD.
- In our finding, we observe that an unstable $(m \geq 0, n = 0)$ finite frequency spontaneously generated acoustic mode, non-linearly couples with itself to drive the TAM mode.
- The frequency of both the observed modes, $\propto \frac{1}{\sqrt{M_i}}$; M_i is the mass of the ion. Thus confirming the acoustic-like nature of the observed mode. [**Umesh Kumar, Physics of Plasmas, 26, 072307 (2019)**]

Unresolved issues

- The exact nature and origin of the driver mode is not known.
- The reason for high frequency of TAM is not known yet.
- The nonlinear interaction shows energy conservation i.e, $\omega_1 + \omega_2 = \omega_3$ but not momentum conservation $k_1 + k_2 \neq k_3$. The reason for this not clear. It indicates that the observed TAM mode is not a normal mode [**Zhang (2009)**, **Fu (2011)**, **Qiu (2017)**].
- The detailed theoretical or numerical explanation of the observed phenomenon is not yet attempted.

Thank you

Bonus slides

Geodesic curvature

- For a curve $f = f(s)$ on a surface C has normal curvature κ_N and geodesic curvature $\kappa_G = \ddot{f}.\frac{\hat{n}\times\dot{f}}{|\dot{f}|^3}$.
- In BETA, magnetic field lines are characterized by $f(s) = (Rcos(s), Rsin(s), 0)$; implies $\kappa_G = 0$.
- For a helical field lines, $f(s) = (Rcos(s), Rsin(s), s)$; again $\kappa_G = 0$.
- As applied vertical magnetic field varies as a function of (R, Z); $f(s) = \left(Rcos(s), Rsin(s), h(s)\right)$ where $h(s)$ could be a function deciding helical nature as well as non-uniformity of the pitch.
- $\kappa_G = \frac{\ddot{h}}{[1+\dot{h}^2]^{\frac{3}{2}}}$; if $h(s) = as + b$ it implies $\kappa_G = 0$. For BETA, h(s), could be a nonlinear function in s which determines the geodesic curvature.

Geodesic curvature

However, in BETA, there are 3 important effects which contribute to nonunifrom pitch to the helical field lines on "surface" $\mathcal{C}$: (a) Toroidal field coils are not perfectly aligned (b) The current-leads used to pass electric current through the toroidal field coils are not fully compensated - resulting in "opening up" of B-field lines to form a irregular helical curve (c) The vertical field applied varies as function of (R, Z) - weaker function of R as compared to Z. The above said reasons provide a nonzero $\ddot{f}(s)$ resulting in a finite geodesic curvature k_G at each (R, Z, ϕ) at a given $R-$surface (i.e, $\mathcal{C}$) as one moves along Z or along toroidal variable φ. Consequently, in general, one may write $f(s)$ as $f(s) = (R\cos(s), R\sin(s), h(s))$ where $h(s)$ could be thought of as a function deciding the helical nature as well as the non-uniformity of the pitch. Thus, one can write, in general, an expression for geodesic curvature κ_G as $\kappa_G = \frac{\ddot{h}}{[1+\dot{h}^2]^{3/2}}$. For example, if $h(s) = as + b$, helical lines with uniform pitch, then $\ddot{h} = 0$ and hence $\kappa_G = 0$! As discussed in BETA device, due to nonuniform vertical field structure, $h(s)$ is a nonlinear function in s which determines the geodesic curvature κ_G, which is nonzero at each R surface $\mathcal{C}$.

Cross phase and coherence of driver and TAM modes

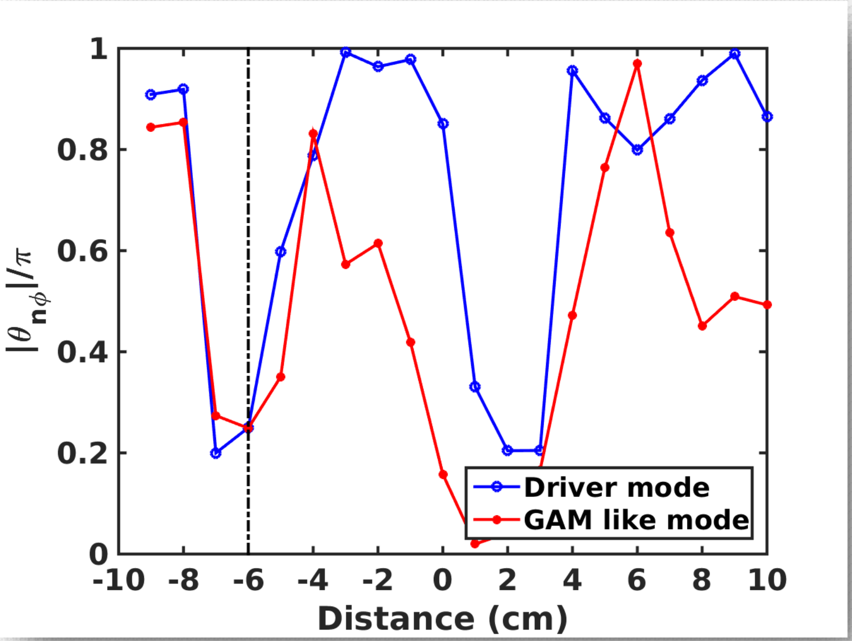

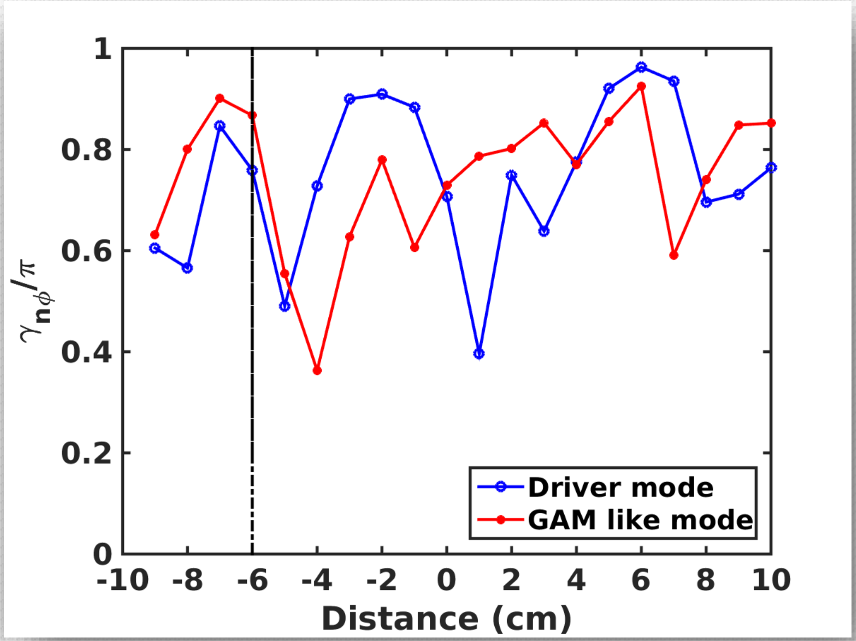

Potential fluctuation spectrogram

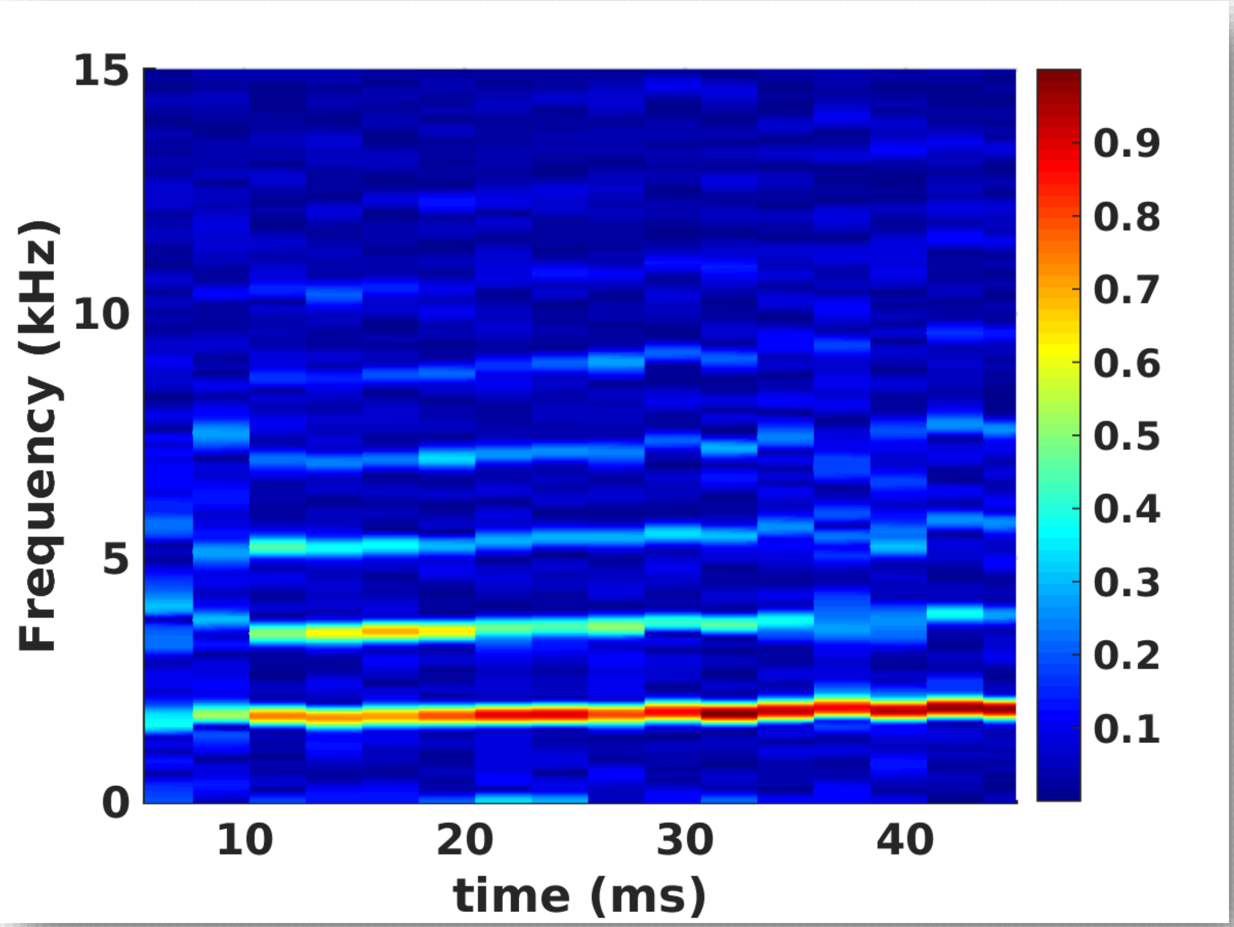

Zoomed in bicoherence plot

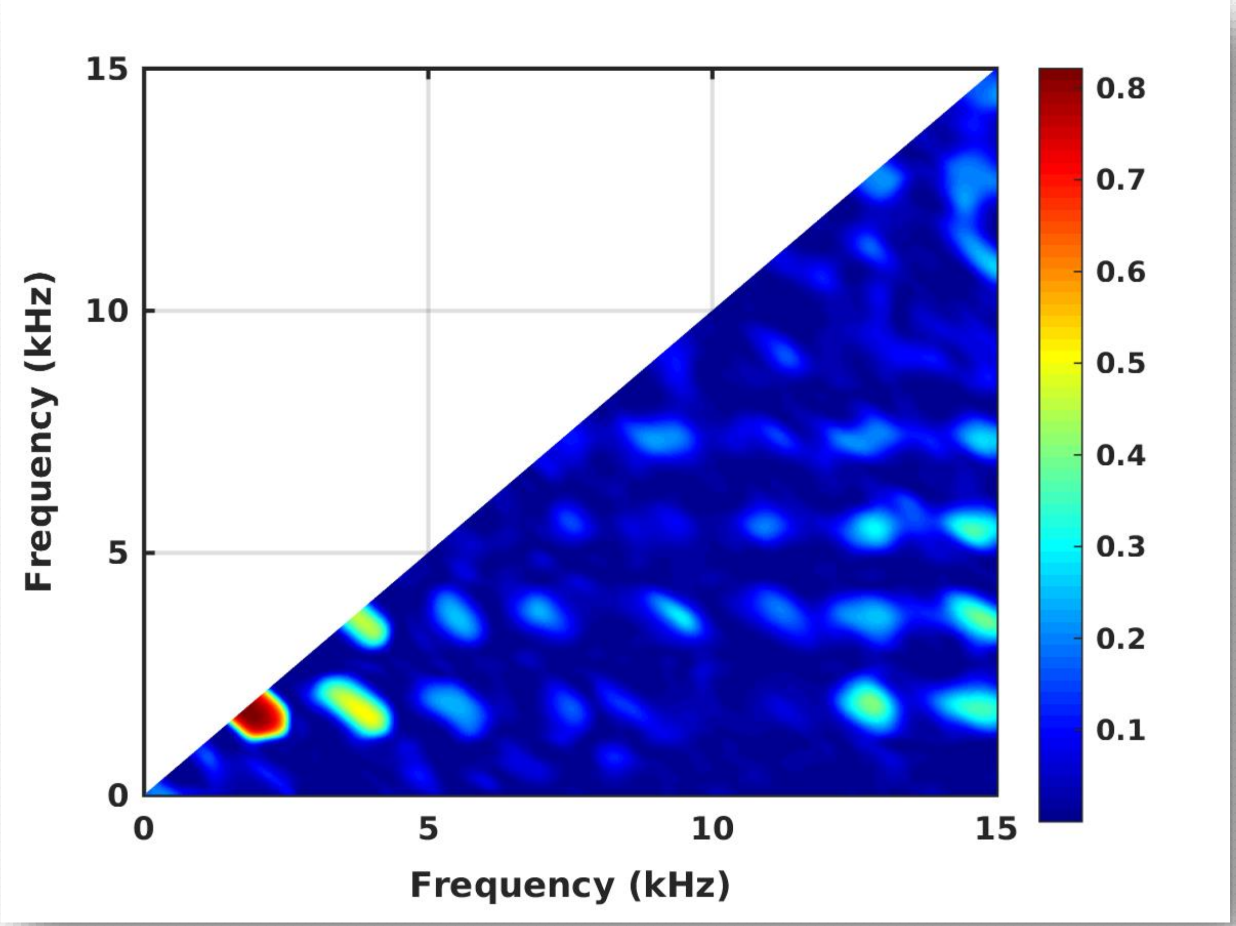

Plasma sources used

Hot cathode source

- A 20 cm long and 2 mm thick tungsten filament is mounted at the minor axis at a particular toroidal location.
- Toroidal fields at the minor axis are 220 G, 330 G, 440 G and 750 G.
- Discharge is struck between wall and hot cathode.
- Discharge current is limited to 5 A and discharge voltage obtained is around 45-50 V.

Microwave source

- Microwave of frequency 2.45 $\pm$ 0.1 GHz in “O” mode is injected from low field side (LFS).
- Toroidal field at the minor axis is around 750 G.
- So electron cyclotron resonance (ECR) lies around -6 cm inboard from the minor axis.
- The upper hybrid (UH) resonance is further facilitates ionization.
- Launched Microwave power is estimated to be around 1 kW.

Experimental parameters

- Working pressure has been kept to 1×10^{-4} torr for all the experiments.
- Mean free path for electron neutral collision (λ_{en}) ~ 1.3 m

$$\lambda_{en} < L$$

where $L = 2\pi R$, R is the major radius.

$$R = 0.45 \text{ m.}$$

Hence plasma is considered to be weakly collisional with respect to the system.

- **At B_T =220 G** $\frac{\nu_{en}}{\omega_{ce}} << 1$ and $\frac{\nu_{in}}{\omega_{ci}} < 1$,
- $\frac{r_{Le}}{a}, \frac{r_{Li}}{a} << 1$, where a = 0.15m (minor radius)

Hence both ion and electrons are magnetized with respect to the system size.

- At **750 G**, ions are electrons both are collision-less.

Determination of topology of toroidal magnetic field

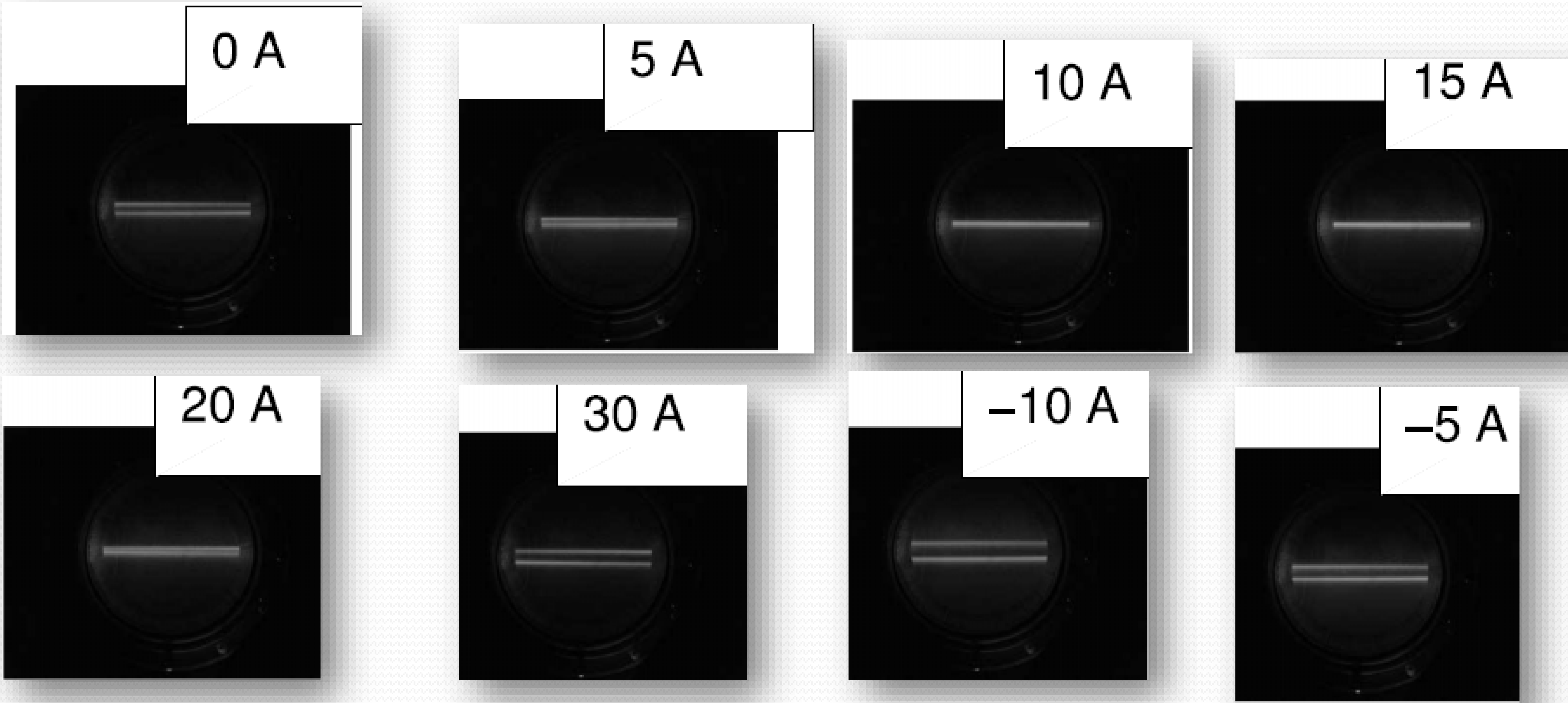

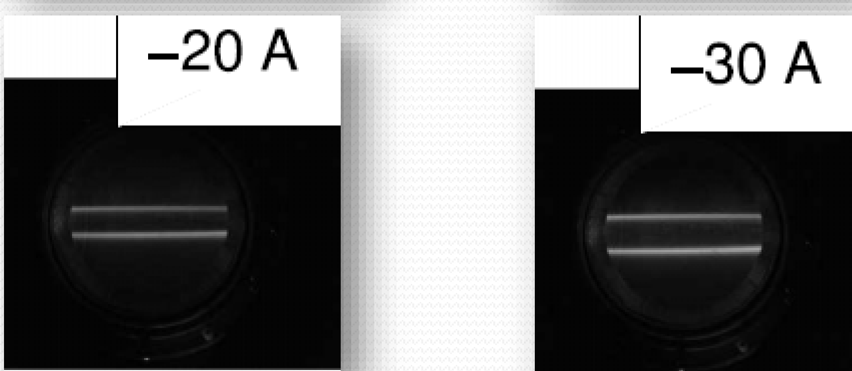

S. G. Thatipamula, Umesh Kumar et al, Rev. Sci. Instrm, 86, 033504 (2015)

Determination of parallel wavenumber

- Probe-1 and probe-2 are aligned on the same toroidal field line.
- Both probes are rotated in the steps of 10^o to find out dip in the floating potential for each VF current.
- During regular discharges both probes aligned to the same height as determined earlier.
- Probe-1 is kept fixed and probe-2 is rotated to find the maximum coherence between two probes.
- $k_{II}^{min} = \frac{\Delta\theta}{\Delta x}$; where $\Delta\theta$ is the cross phase between probe-1 and probe-2 and $\Delta x = \frac{2\pi R}{4} = 0.75\ m$ is the probe separation.

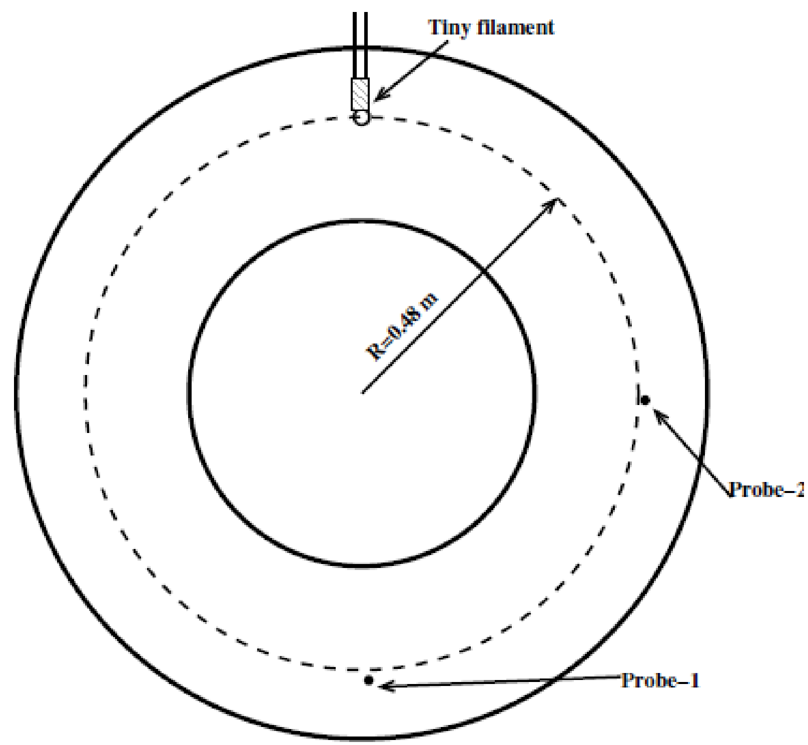

Numerical simulation of magnetic field

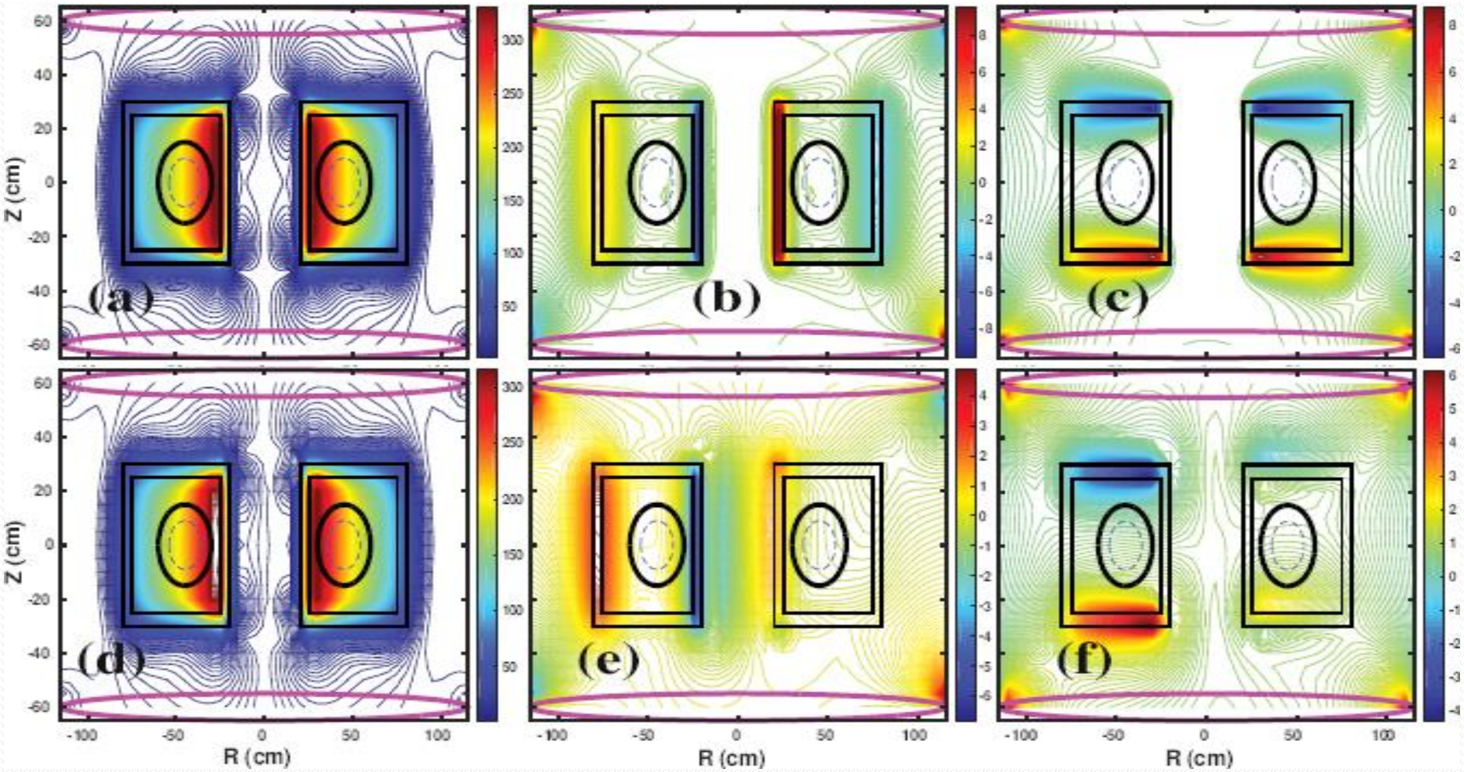

- Contour plots of (a) B_T, (b) B_r, (c) B_v for the ideal case, and (d) B_T, (e) B_r, (f) B_v for the actual co-ordinates of TF coils for BETA for an external VF current of 12 A.
- The magnetic field data is obtained using the EFFI simulation for the ideal and the actual case (Thanks to Mrs. Richa Bandopadhyay and Mr. Sharvil Patel)

Simulated radial profile of vertical magnetic field

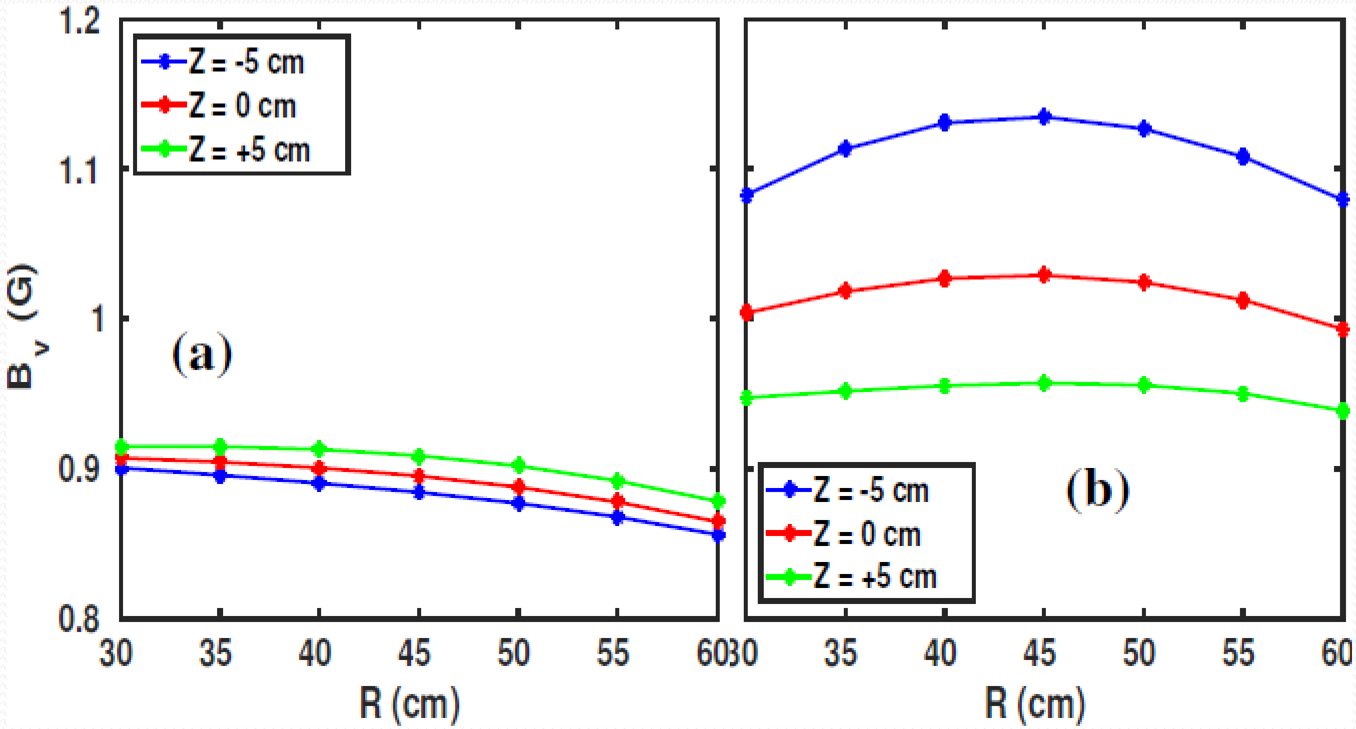

- Radial profile of vertical magnetic field B_v; (a) an ideal TF locations and (b) the actual TF locations at different vertical distance Z for the case when VF coils are charged to 12 A current.
- It can be observed that for the ideal case shown in (a) has very weak dependency on Z as compared to the actual case (b).

Topology of toroidal field line

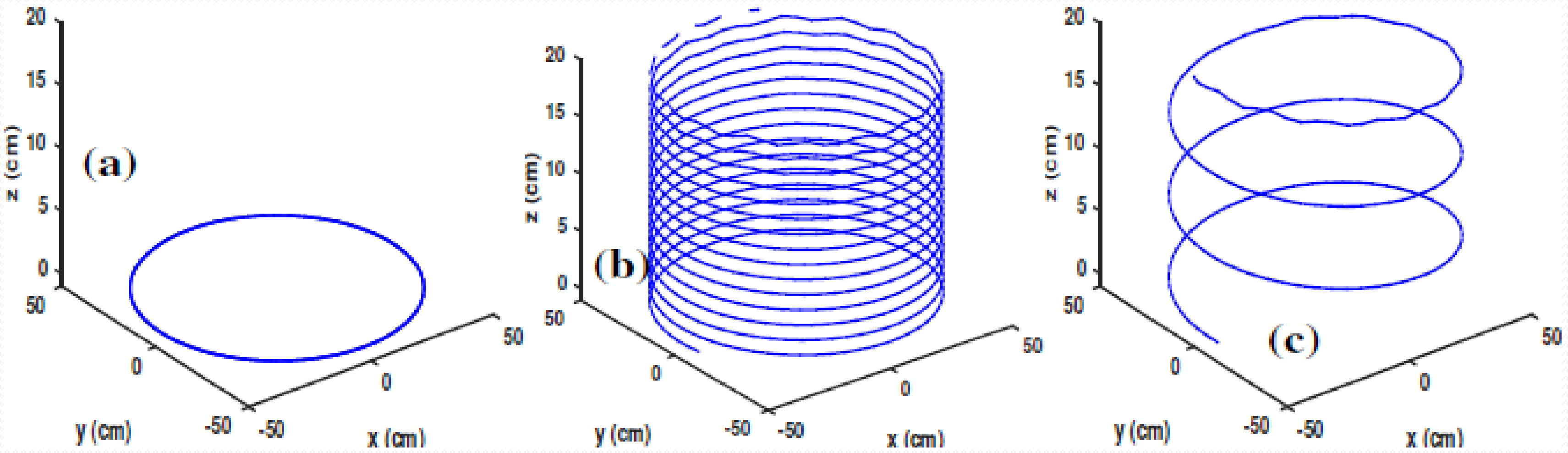

- The topology of the toroidal field in Cartesian co-ordinates for actual TF coils locations simulated using EFFI code for VF currents of (a) 0 A or uncharged VF coils, (b) 12 A and (c) 60 A.
- It can be observed that for 0 A case, the field lines closes on itself despite the geometrical misalignment in the TF coils.
- The simulation does not consider the generation of offset magnetic field due to uncompensated current leads.

Operating conditions

- Base Pressure ~ 5.0×10^{-6} torr
- Filament current ~ 142 A.
- Discharge current ~ 5 A.
- Filling gas :- Argon
- Working pressure ~ 1.0×10^{-4} torr
- Toroidal Magnetic field coil current~ 1 kA for 220 Gauss at the minor axis.
- Vertical magnetic field coil current ~ 0 A, 12 A (~ 1.0 Gauss), 20 A (~1.5 G), and 60 A (~4.5 G).

Mean plasma profiles

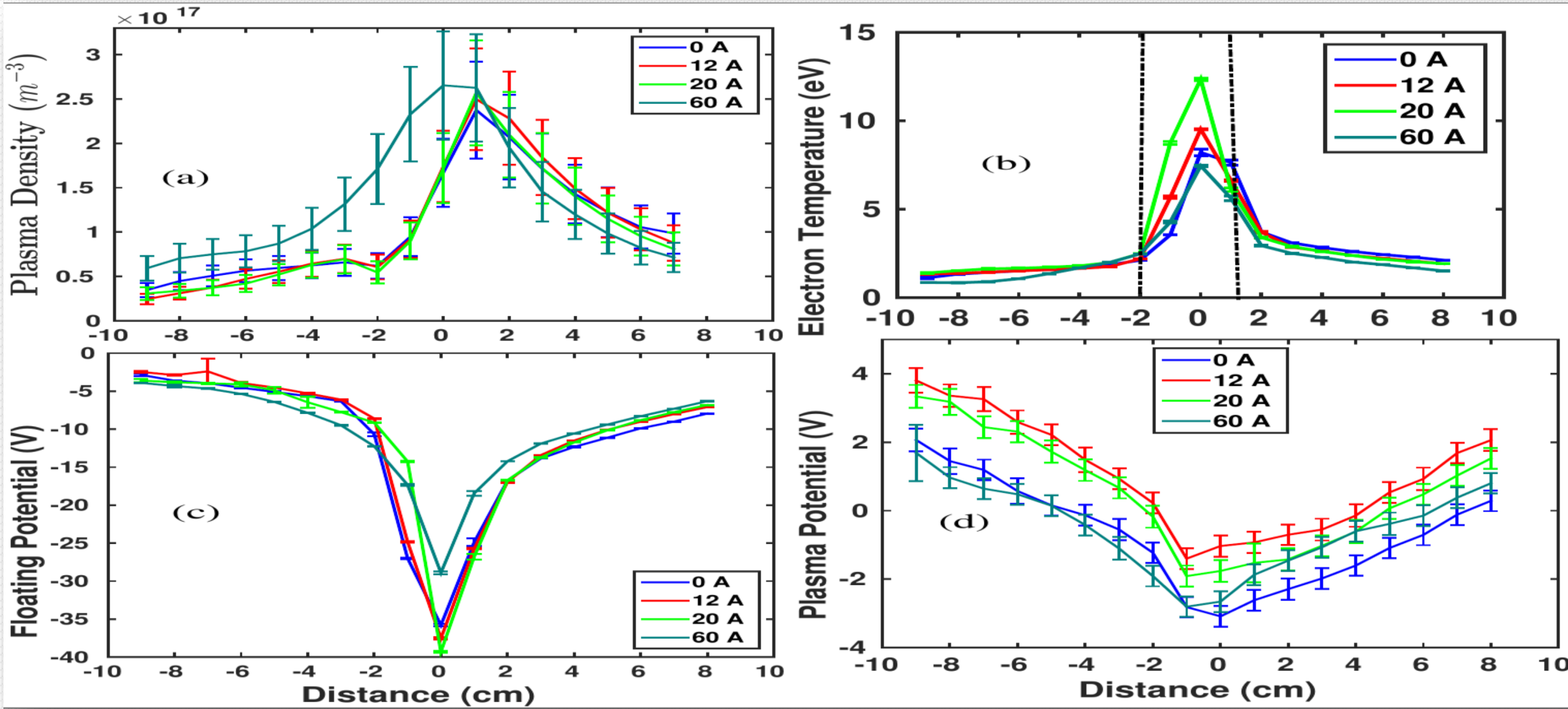

- Radial profiles of (a)density, (b)electron temperature, (c) floating potential and (d) plasma potential are shown here.

•Density for widely opened field line or small L_c higher than other values on inboard side.

•Large dip in floating potential and peak in temperature around minor axis is due to presence of high energy electrons around minor axis.

Power spectrum

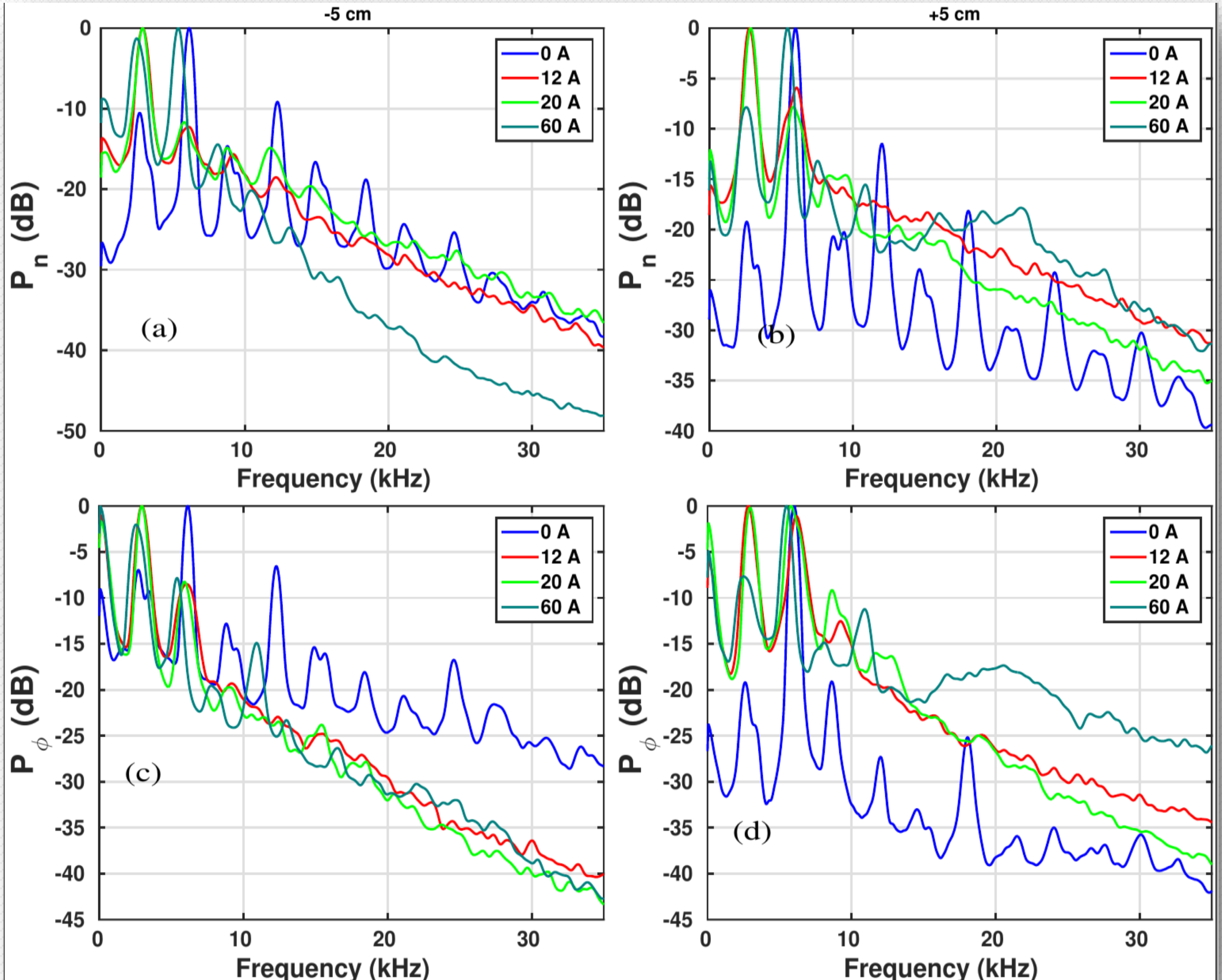

- Auto power spectra for (a) density at -5 cm, (b) density at +5 cm, (c)potential at -5 cm, and (d) potential at +5 cm for four different values of vertical field coil current.

- Though sampling frequency is 200 kHz, but all these plots zoomed in to 35 kHz only.

Bispectrum

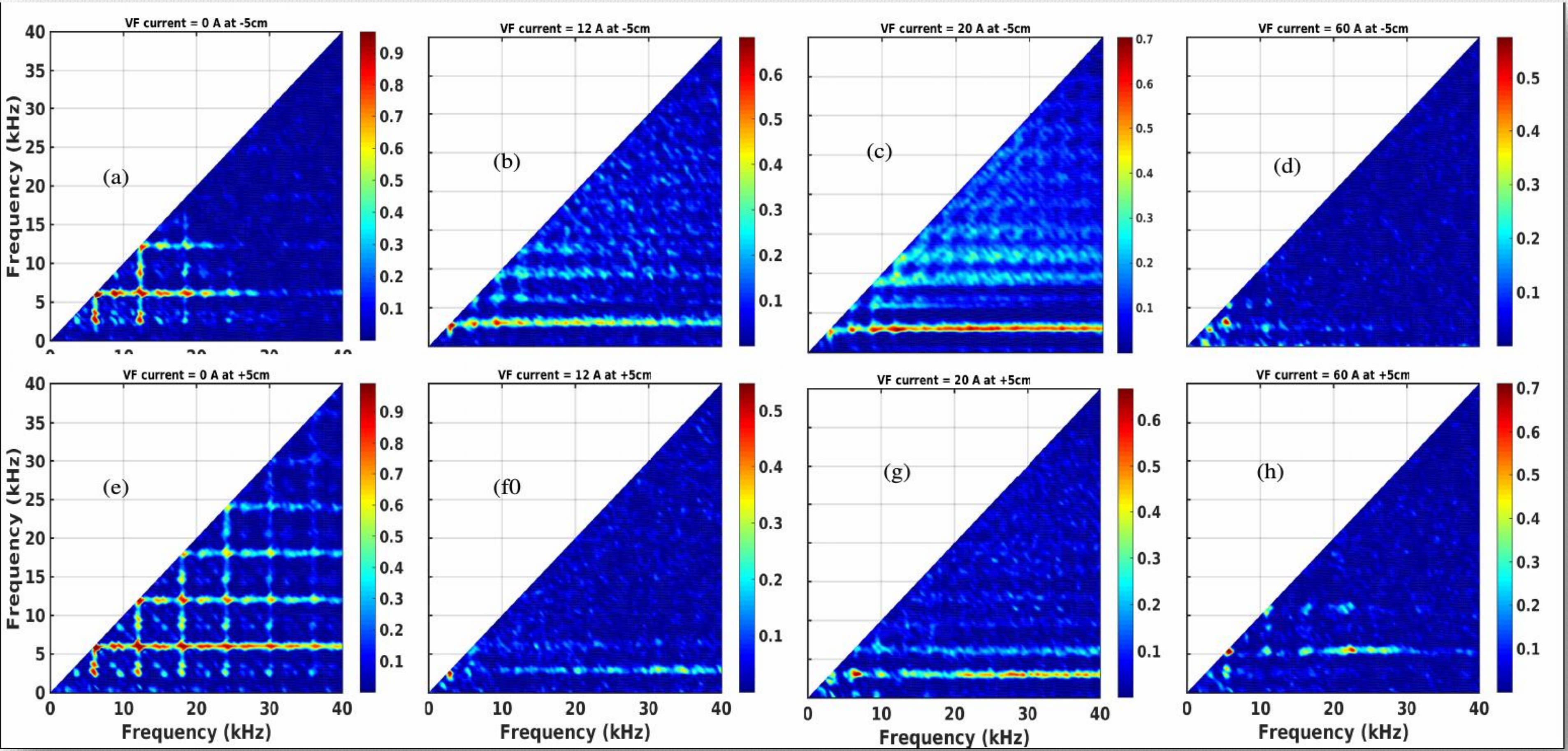

Bispectrum of I_{sat} fluctuation for single shot for VF current of 0A, 12A, 20A, and 60A at -5 cm and +5 cm. $b^2 > 0.9$ for 0A and reduces further for higher currents. These plots are zoomed in up to 40 kHz.

S(k,ω) and wavenumber

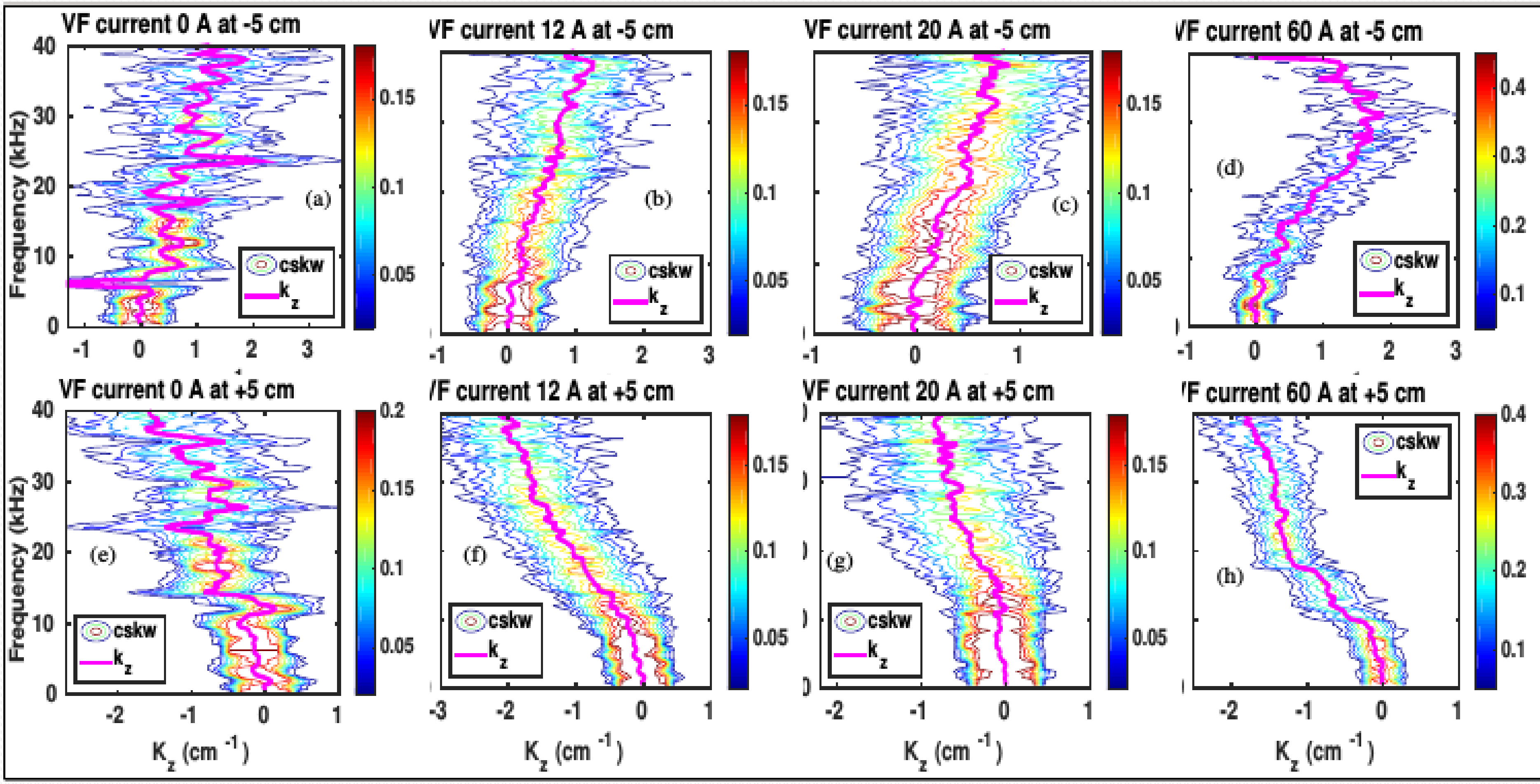

Contour plots of conditional spectrum S(k,ω) with embedded line showing vertical wavenumber (k_z *or* k_θ) estimated four VF currents at -5 cm and +5 cm.

Net poloidal flow

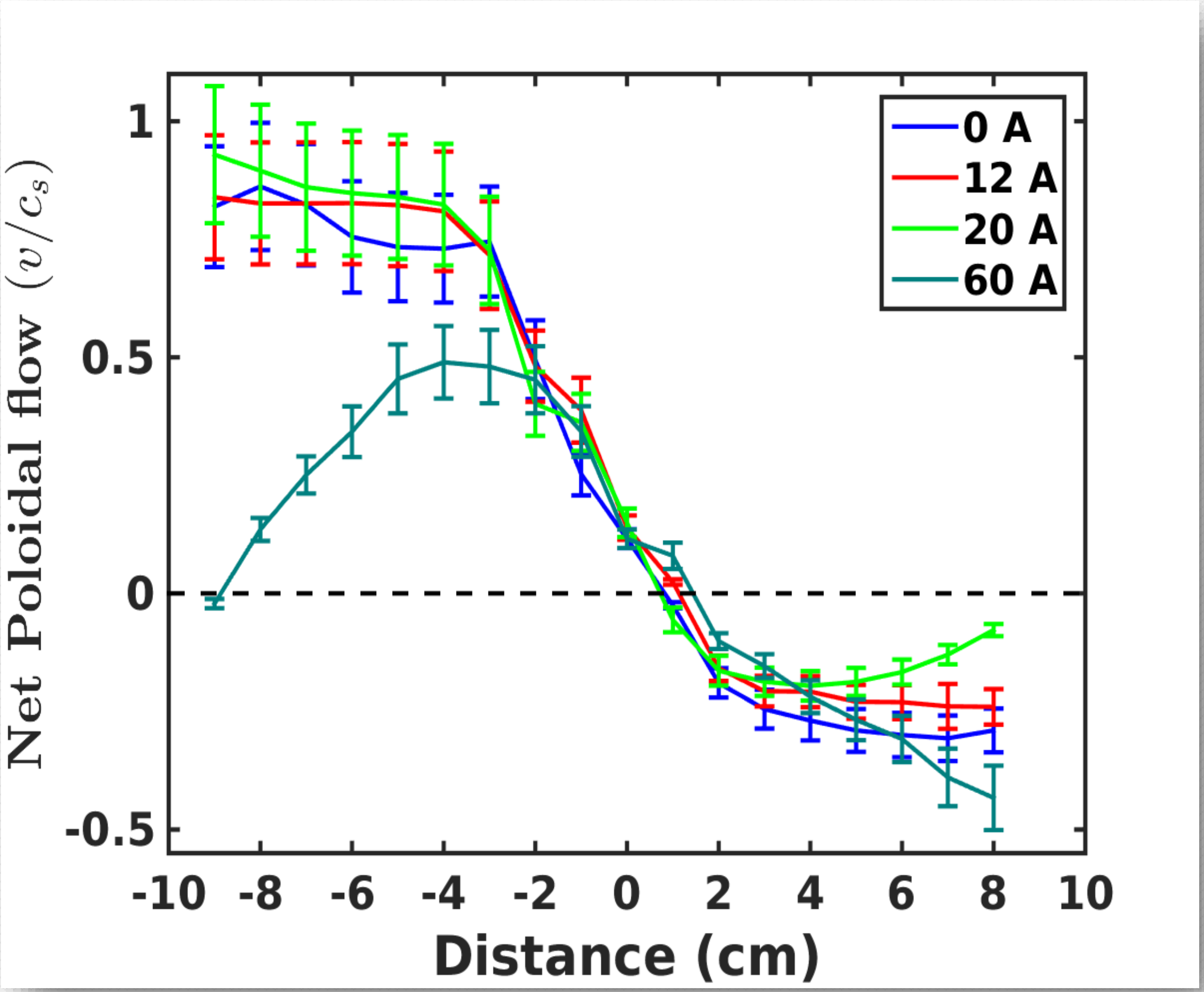

- Radial profile of net poloidal flow measured using Mach probe for four values of the VF coil current.
- The net poloidal flow increases slightly for 12A and 20A cases on HFS, but reduces to nearly zero for 60A case on inboard side close to limiter.

Identification of instabilities

Instability	Necessary Condition	Frequency ω $\omega_D = k_z(\frac{T_e}{BL_n})$	$k_{\|\|}$	$\theta_{n\phi}$	$\frac{\frac{e\widetilde{\phi}}{K_B T_e}}{\frac{\widetilde{n}}{n_0}}$
Rayleigh-Taylor (RT)	$\vec{g}.\vec{\nabla}n < 0$ $\frac{\nu_{en}}{\omega_{ce}} < 1,\ \frac{\nu_{in}}{\omega_{ci}} < 1$	$0.5\left(\frac{2L_n}{R} - \frac{T_i}{T_e}\right)\omega_D$	≈ 0	$\frac{\pi}{2}\ to\ \pi$	≥ 1
Kelvin Helmholtz (KH)	$\overrightarrow{V_E}' \neq 0$ $\vec{\nabla}n \neq 0$ (modifies KH)	$\sim k_\perp V_E$	≈ 0	$\frac{\pi}{2}\ to\ \pi$	$\gg 1$
Drift like	$\vec{\nabla}n \neq 0$	$\sim \omega_D$	$\neq 0$	$0\ to\ \frac{\pi}{4}$	≤ 1
Simon Hoh (SH)	$\vec{E}.\vec{\nabla}n > 0$ $\frac{\nu_{en}}{\omega_{ce}} < 1,\ \frac{\nu_{in}}{\omega_{ci}} \leq 1$	$\frac{T_i}{2T_e}\omega_D$	≈ 0	$\frac{\pi}{2}\ to\ \pi$	≥ 1
Modified Simon Hoh (MSH)	$\vec{E}.\vec{\nabla}n > 0$ $\frac{\nu_{en}}{\omega_{ce}} < 1,\ \frac{\nu_{in}}{\omega_{ci}} < 1$	$\frac{T_i}{2T_e}\omega_D$	≈ 0	$\frac{\pi}{2}\ to\ \pi$	≥ 1

Cross phase and coherence

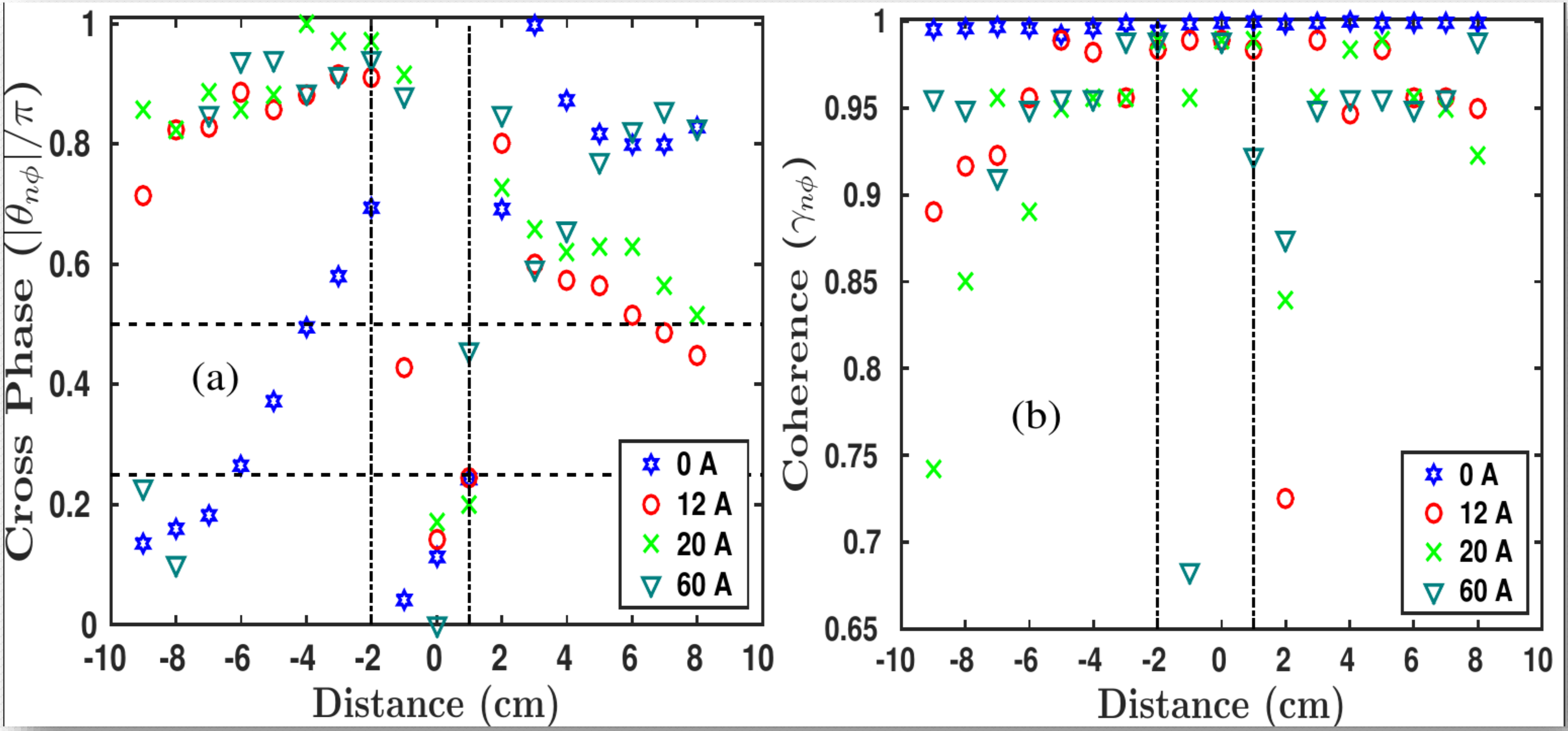

- Cross phase normalized to of density and potential fluctuations and Coherence between density and potential for four values of VF current of 0 A, 12 A, 20 A and 60 A.
- Coherence is more than 0.7 for all VF current.
- Outboard side is dominated by flute like instabilities.

Ratio of potential fluctuation to density fluctuation

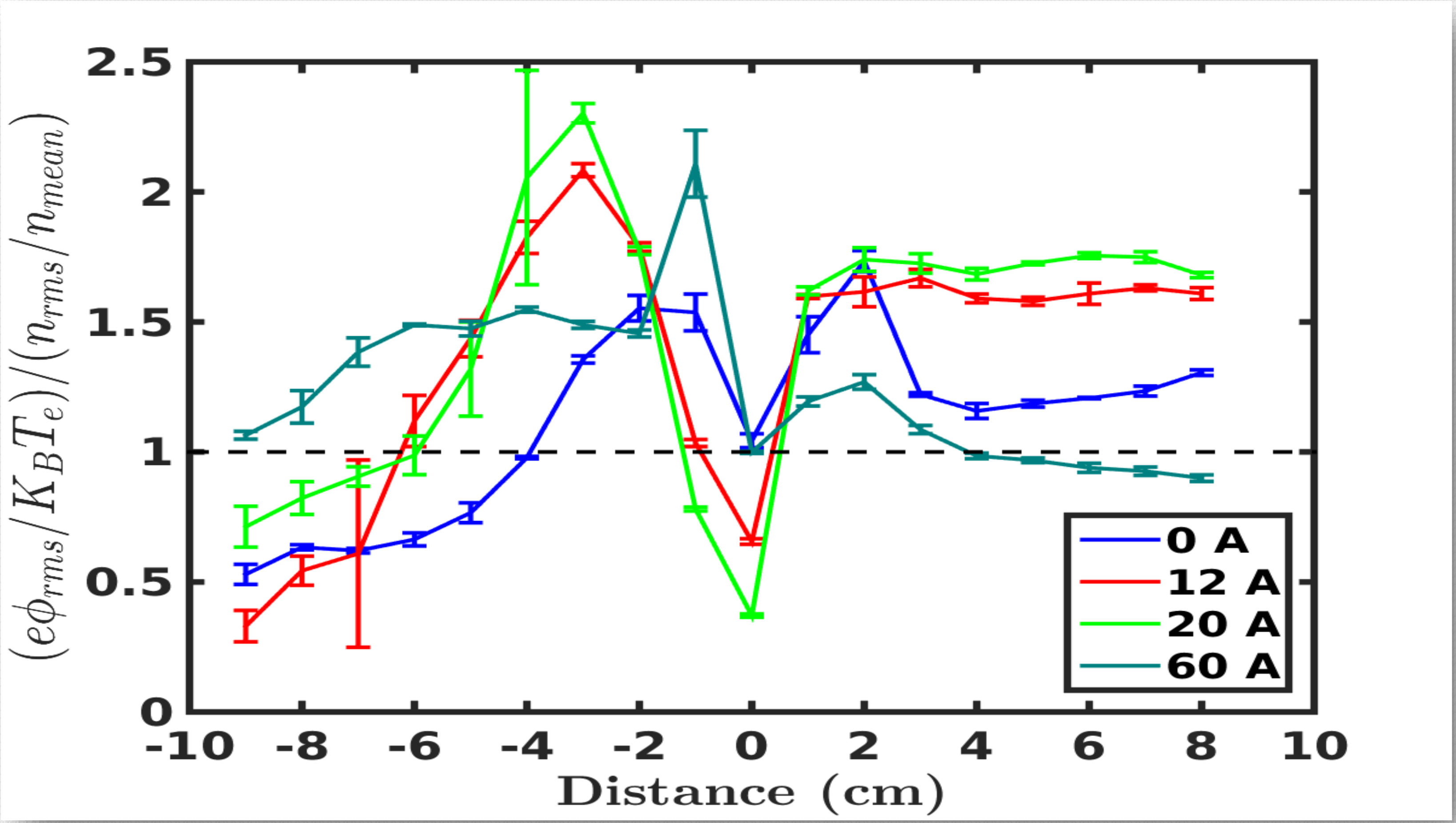

- Radial profile of ratio of relative potential fluctuations to relative density fluctuations. On HFS for 0 A case the value ranges from 0.5 to 1, but for 12 A and 20 A case it goes from 0.2 to 2.2 which shows presence of shear instabilities.

Summary:- ch-4-I

- L_c strongly controls the equilibrium plasma profiles like density, temperature and potential.
- for small L_c a broad band exist for higher frequency on the outboard side.
- Strong non-linear interaction exist for 0 A, 12 A and 20 A and interaction of dominant modes with background fluctuation is present.
- Net poloidal flow tends to zero for small value of L_c on inboard side close to the limiter.
- Flute like instabilities are dominant on the outboard side.
- Velocity shear is dominant for the all VF values except 60 A, where net poloidal flow is strong.

Mean density profile

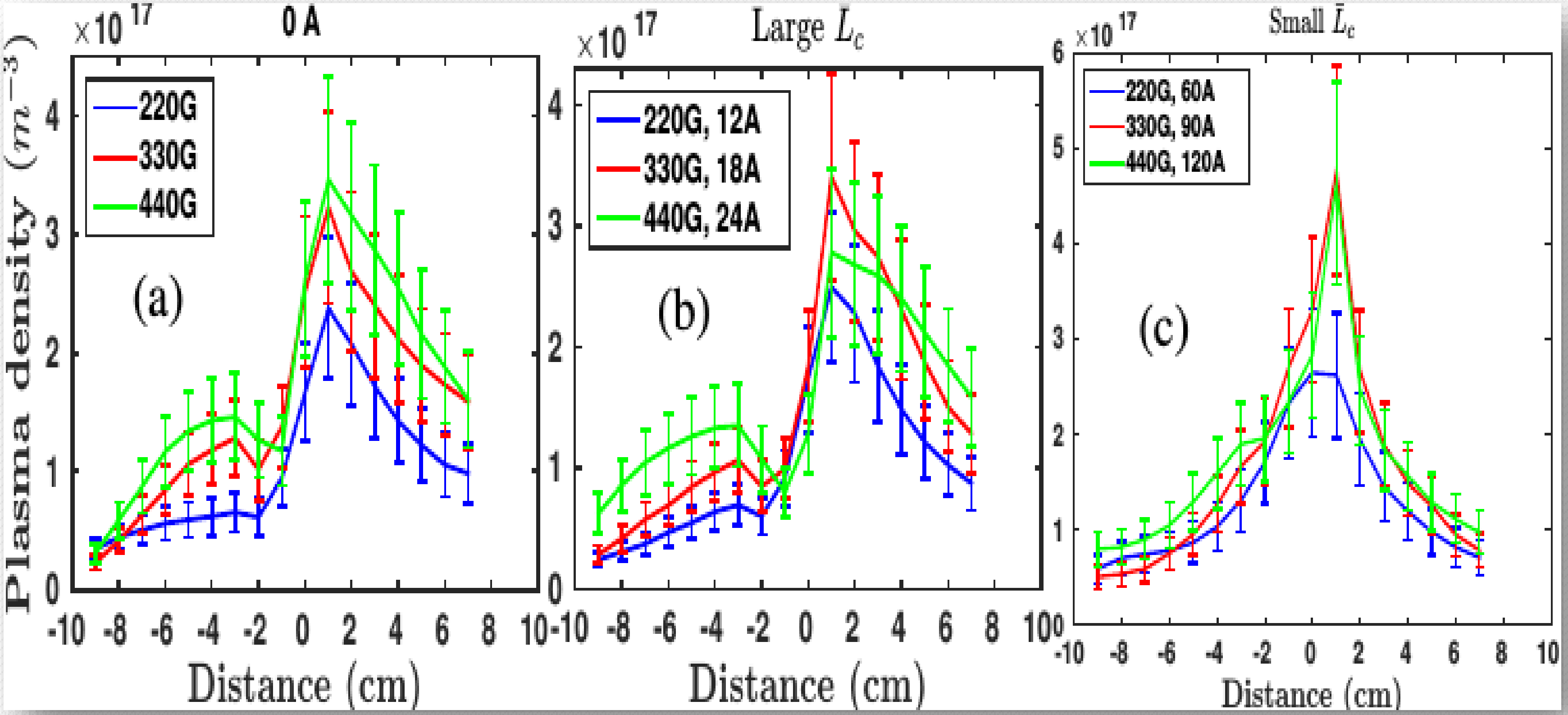

- Plasma density with simultaneous variation in B_v *and* B_T in fixed ratios.
- Densities are symmetric around minor axis for small L_c case, could be due to effective short-circuiting of the E_z.

Power spectrum of density fluctuation

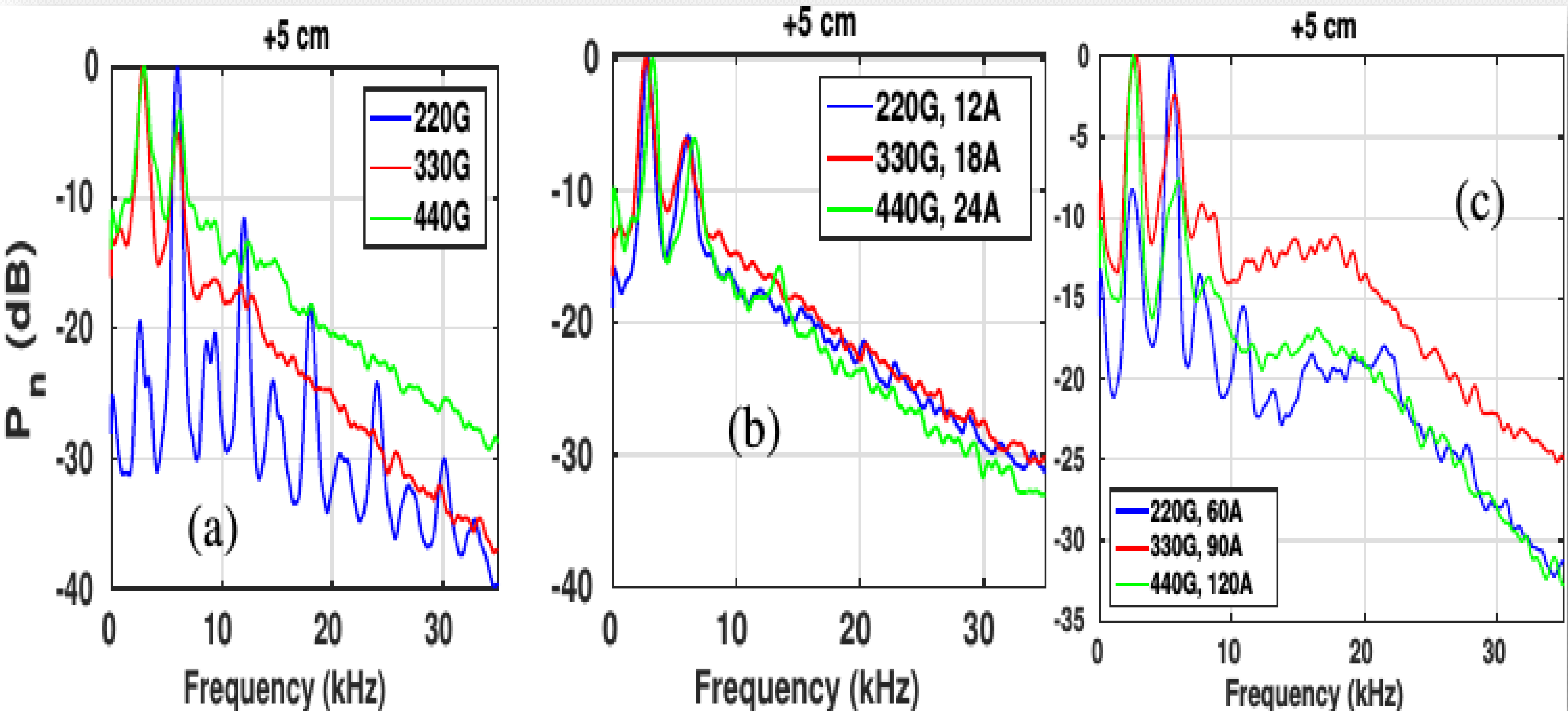

- Density fluctuation with simultaneous variation in B_v *and* B_T in fixed ratios.
- A broad band can be observed for small L_c cases.

Conclusion:- ch-4 (I & II)

- L_c strongly controls the equilibrium plasma parameters. [I & II]
- Density increases on inboard side for smaller L_c . [I & II]
- Large L_c has few modes followed by turbulent background and small L_c shows broad band for background fluctuations. [I & II]
- For small L_c net flow tends to zero on the inboard side. [I]
- Outboard side is dominated by R-T kind of instabilities and inboard side shows shear driven fluctuations. [I]
- Poloidal flow generates velocity shear which facilitates generation of shear driven instabilities on the inboard side. [I]

Mean ECR plasma profiles

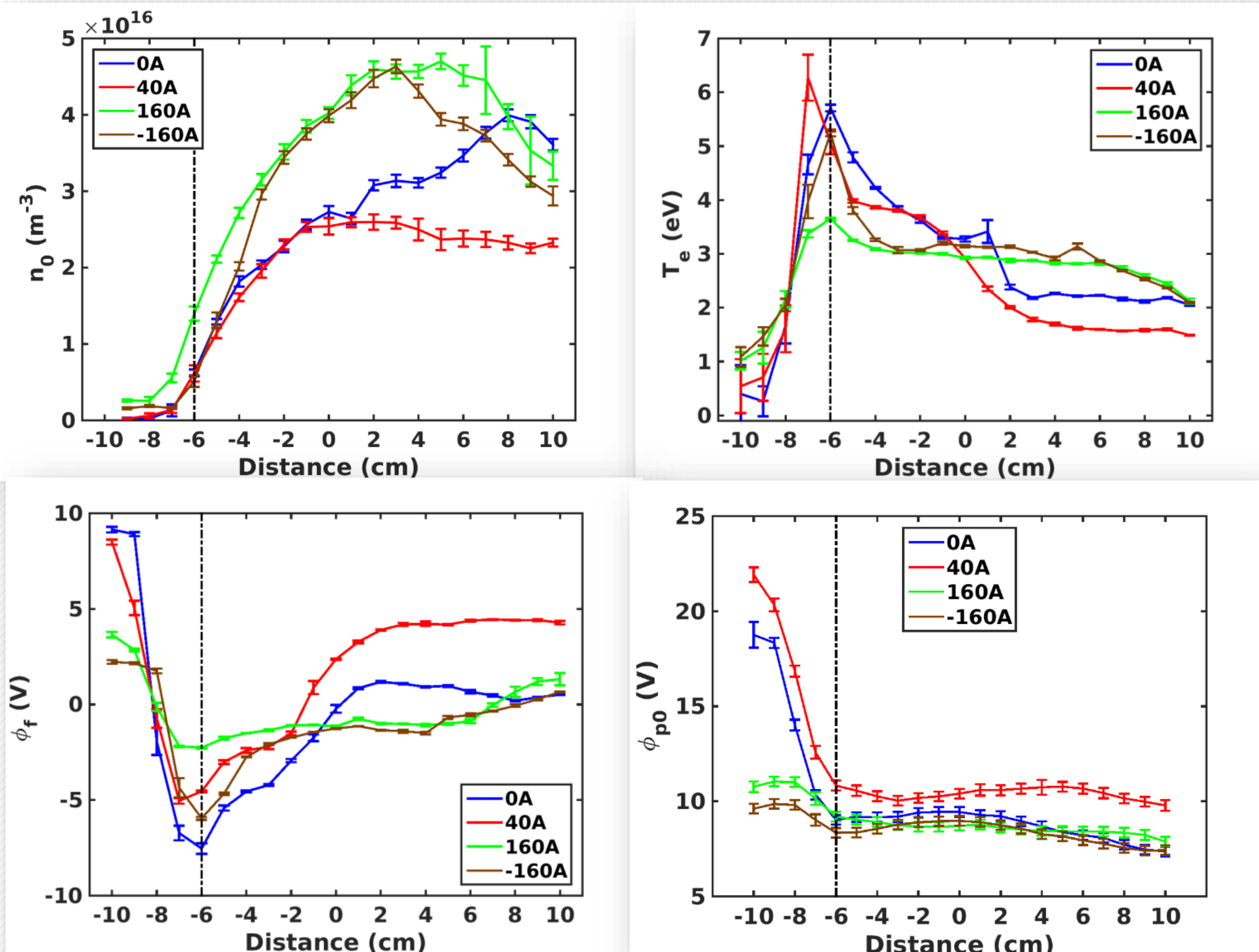

- Mean profile for ECR source with varying B_v.
- The vertical line at -6 cm is the EC region.
- The EC region coincides with peak in temperature and dip in potential.
- The $\frac{v_{E_Z \times B}}{a}$ is compared with ionization rate, ν_{iz}.
- It has been observed that $\nu_{iz} \gg \frac{v_{E_Z \times B}}{a}$.

Resonances

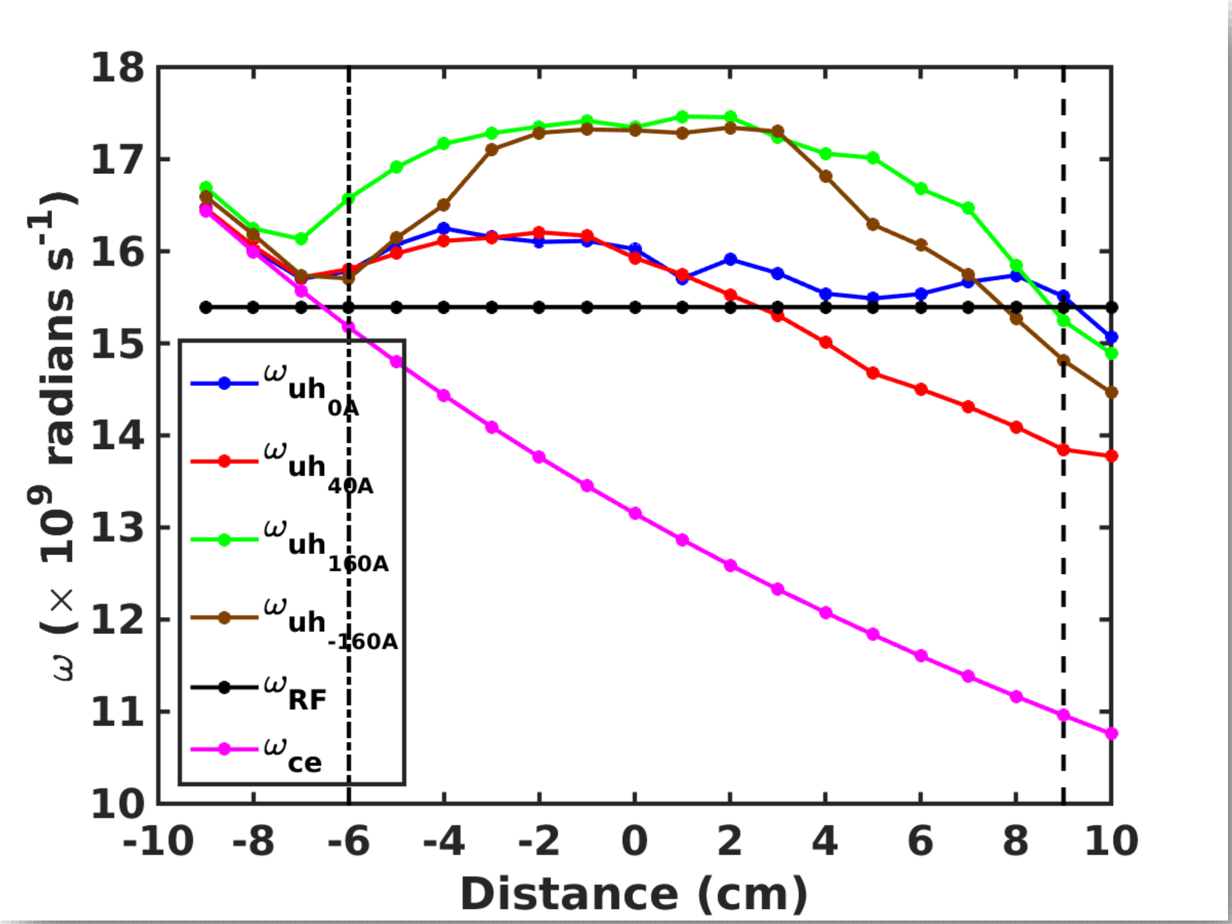

- Radial profile of the upper hybrid resonance for different VF current.
- $\omega_{UH}(r) = \sqrt{\omega_{ce}^2(r) + \omega_{pe}^2(r)}$
- The vertical line at -6 cm is due to ECR ionization.
- Secondary ionization occurs due to UH resonance.
- The location of UH varies with VF current.

Power spectrum of density fluctuation

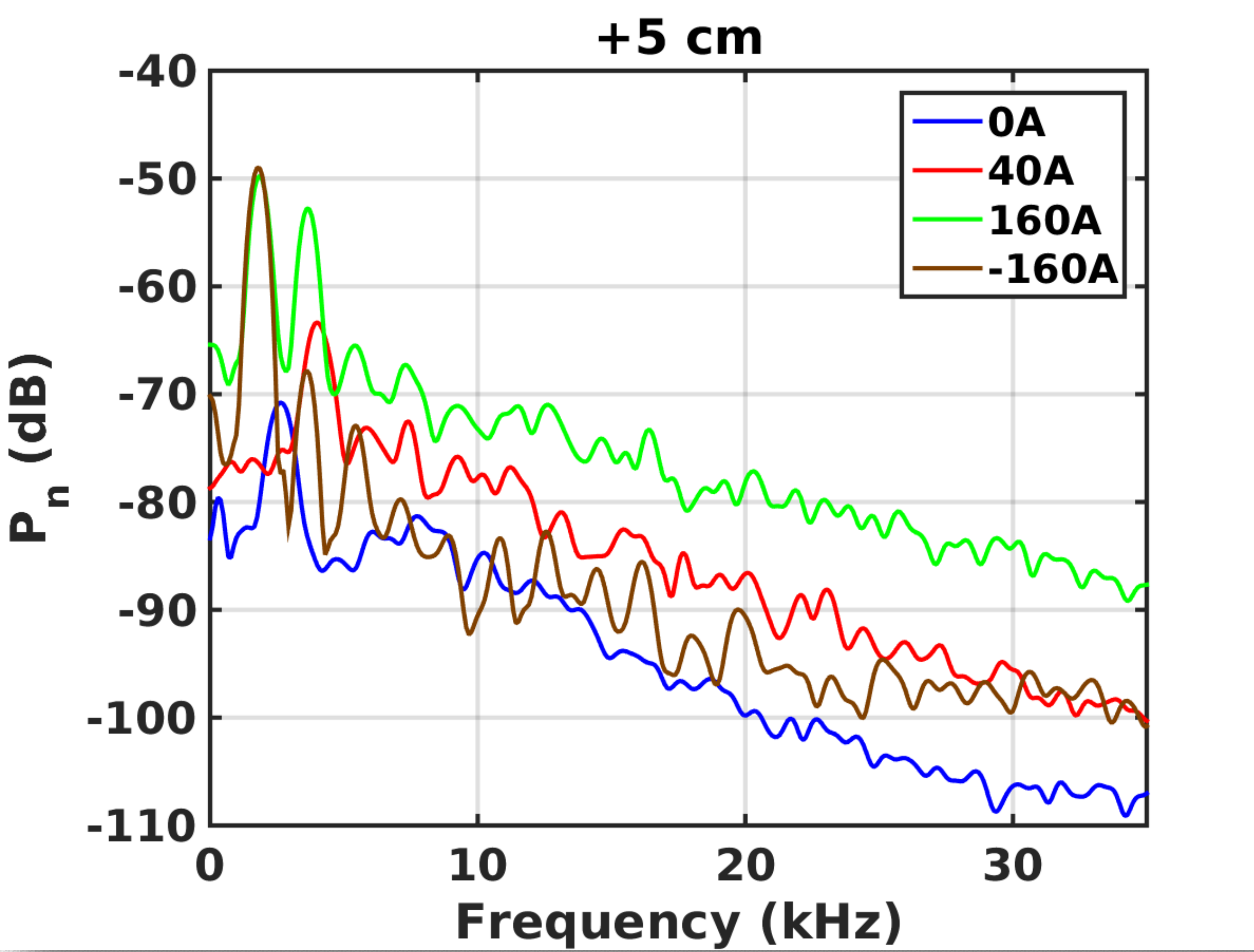

- Power spectrum of density at r=+5 cm.
- For each B_v, there exist, one or two dominant mode followed by background fluctuations.
- The dominant mode lies in the range of 1.7 kHz to 4 kHz.

Net poloidal flow

Hot cathode

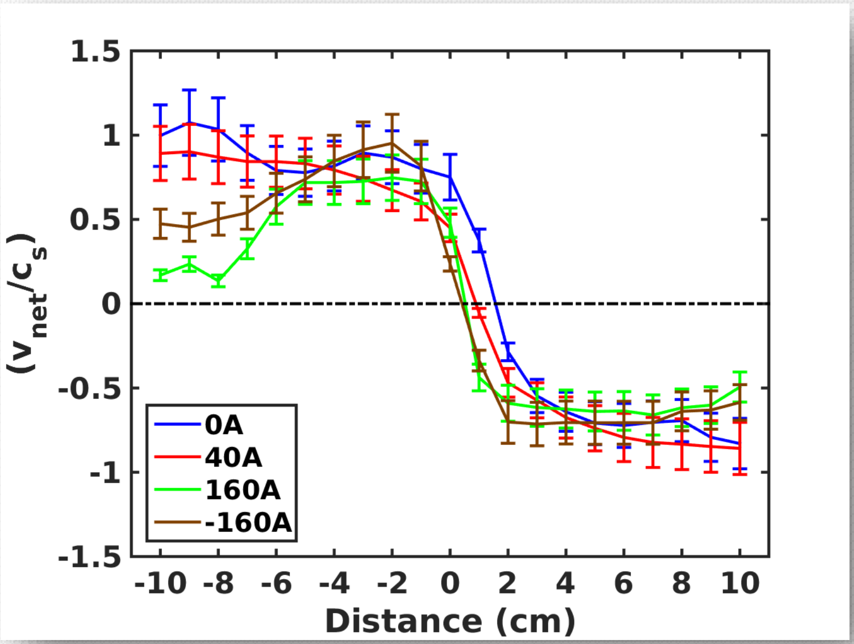

ECR source

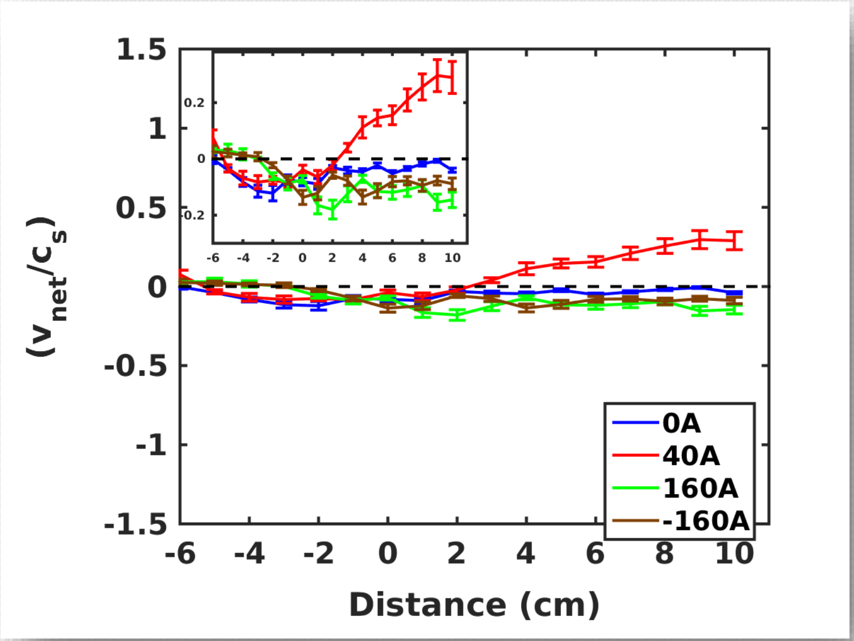

- The density for hot cathode plasma is around 5 times more than the ECR plasma.
- The toroidal flow measured to be around $\pm 0.1 c_s$ and hence negligible.
- The net flow for hot cathode source is very strong as compared to ECR source.
- The horizontal line represents for zero net poloidal flow.

Particle confinement for 40 A

Hot cathode plasma

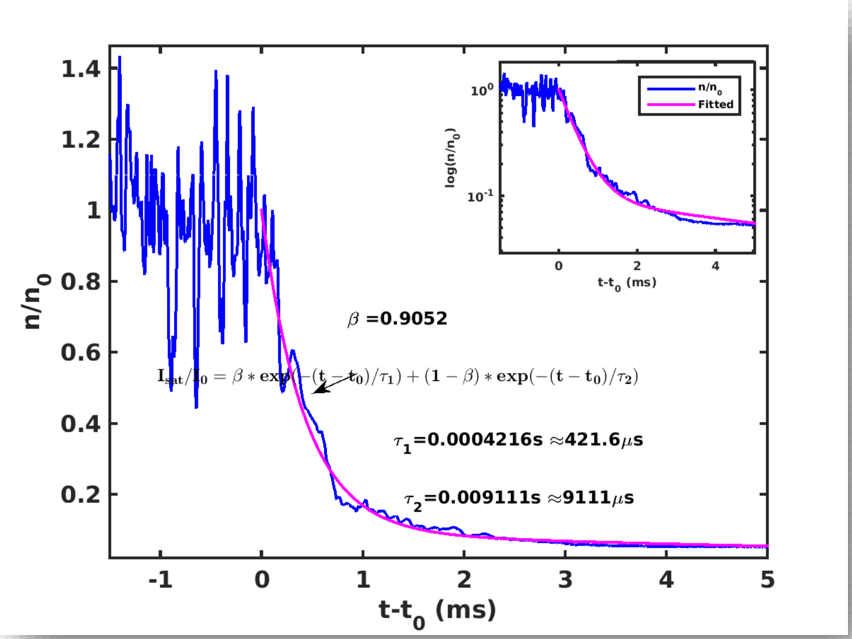

ECR plasma

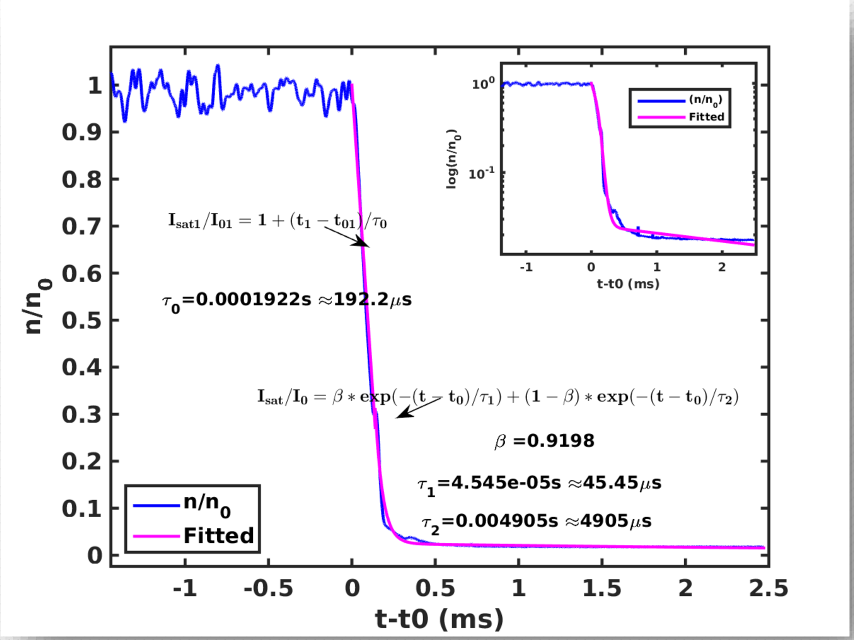

- Density fall for hot cathode source for 40 A or large connection length case.
- Density shows exponential fall, after the source is turned off.

- Density fall for ECR source for 40 A or large connection length case.
- Density shows linear followed by exponential fall, after the source is turned off.

Particle confinement for 160 A

Hot cathode plasma

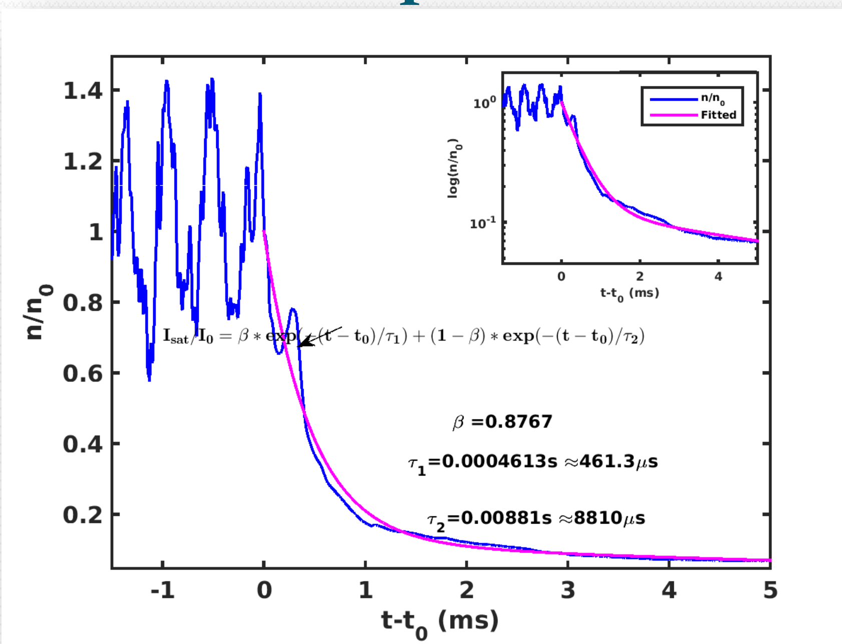

ECR plasma

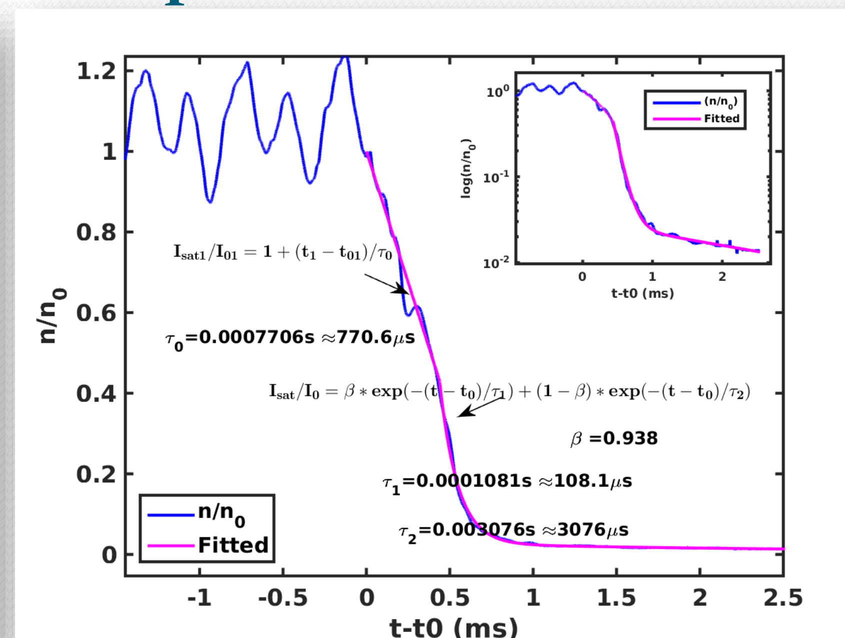

- Density fall for hot cathode source for 160 A or short connection length case.
- Density shows exponential fall, after the source is turned off.

- Density fall for ECR source for 160 A or short connection length case.
- Density shows linear fall followed by exponential fall, after the source is turned off.

Comparison of particle confinement time for two sources at $B_T = 750\ G$ at the minor axis

VF Current (A)	Hot cathode source			Microwave source			
	$\boldsymbol{\beta}$	$\boldsymbol{\tau_1}$ **(ms)**	$\boldsymbol{\tau_2}$ **(ms)**	$\boldsymbol{\tau_0}$ **(ms)**	$\boldsymbol{\beta}$	$\boldsymbol{\tau_1}$ **(ms)**	$\boldsymbol{\tau_2}$ **(ms)**
0	0.9433	0.287	19.2	0.214	0.9337	0.021	11.3
40	0.9052	0.422	9.1	0.192	0.9198	0.045	4.9
160	0.8767	0.461	8.8	0.771	0.9380	0.108	3.08
-160	0.8327	0.589	10.1	0.291	0.9456	0.049	7.91